Magnetoencephalographic (MEG) Characterization of Dynamic Brain Activation

Basic Principles and Methods of Data Collection and Source Analysis

Matti Hämäläinen[†] and Riitta Hari
Brain Research Unit, Low Temperature Laboratory,
Helsinki University of Technology, 02015-HUT, Espoo, Finland
†Present address: NMR Center, Massachusetts General Hospital, Boston, USA.

To appear in: Toga et al. (eds) Brain Mapping: The Methods, 2nd Edition

I. Introduction

Timing is essential for proper brain functioning. Magnetoencephalography (MEG) and electroencephalography (EEG) are at present the only noninvasive human brain imaging tools that provide submillisecond temporal accuracy and thus help to unravel dynamics of cortical function. The advantage of MEG over EEG is that skull and scalp, which affect the electric potential distributions, do not smear the magnetic signals and MEG is thus able to see cortical events 'directly through the skull'. MEG (and EEG) reflect the electrical currents in neurons directly, rather than the associated hemodynamic or metabolic effects.

In an MEG study (see Fig. 1), one records with sensitive detectors weak magnetic fields generated by currents in the brain. The aim is to pick up the magnetic field at several locations outside the head and then to calculate the most probable source currents in the brain. MEG is a noninvasive technique well suited for investigation of brain regions embedded within cortical sulci. These cortical areas are poorly accessible even with intracranial recordings but produce an extracranial magnetic field which can be detected with MEG sensors.

Insert Figure 1 about here

The magnetic signals generated by cortical currents are picked up with superconducting coils connected to SQUIDs (superconducting quantum interference devices), the ultrasensitive detectors of magnetic fields. The present state-of-the-art neuromagnetometers contain more than 300 SQUIDs in helmet-shaped arrays so that signals can be recorded simultaneously over the whole neocortex.

Our chapter begins with the discussion of the generation of MEG signals. For this end, a review of the relevant electromagnetic concepts is necessary. Next, we discuss the instrumentation, magnetic shielding, and practical technical aspects of data acquisition and signal processing. We continue with a discussion of several source analysis techniques and conclude with some practical examples of MEG data acquisition and interpretation. More comprehensive information on MEG and its applications in different types of studies can be found in detailed review articles (see, e.g. Hämäläinen *et al.,* 1993; Näätänen *et al.,* 1994; Lounasmaa *et al.,* 1996; Hari 1999; Hari *et al*., 2000) and http://biomag2000.hut.fi/papers_all.html.

II. Generation of Neuromagnetic Fields

A. Sources and Fields

Neuronal currents generate magnetic and electric fields according to principles stated in Maxwell's equations. The neural current distribution can be conveniently described as the primary current, the "battery" in a resistive circuit comprising the head. The postsynaptic currents in the cortical pyramidal cells are the main primary currents giving rise to measurable MEG signals. In many calculations the head can be approximated with a spherically symmetric conductor but more realistic head models for field calculations can be constructed with help of anatomical MR or CT images.

1. Quasistatic Approximation of Maxwell's Equations

The electric field **E** and the magnetic field **B,** induced by the total electric current density, **J**, can be solved from Maxwell's equations. Because **J**, **E**, and **B** vary in time rather slowly (below 1 kHz) (Plonsey 1969; Hämäläinen *et al.,* 1993) the sources and fields can be treated in a quasistatic approximation. Thus inductive, capacitive and displacement effects can be neglected, and the true time-dependent terms in the field equations can be omitted.

In the quasistatic approximation the Maxwell's equations read:

$$\begin{aligned} \nabla \cdot \mathbf{E} &= \rho / \varepsilon_0 \\ \nabla \times \mathbf{E} &= 0 \\ \nabla \cdot \mathbf{B} &= 0 \\ \nabla \times \mathbf{B} &= \mu_0 \mathbf{J} \end{aligned} \qquad (1)$$

where ρ is the charge density and ε_0 and μ_0 are the permittivity and permeability of vacuum, respectively. Particularly, it is seen from the last of the Eqs. (1) that the magnetic field is produced by the total electric current density **J**.

2. Primary Currents

It is useful to divide the total current density, **J**, into two components. The passive volume or return current is proportional to the conductivity (σ) and the electric field (**E)** so that $\mathbf{J}_v = \sigma\mathbf{E}$. $\mathbf{J}_v$ is the result of the effect macroscopic electric field on charge carriers in the conducting medium. Everything else is the primary current $\mathbf{J}_p$:

$$\mathbf{J}_p = \mathbf{J} - \sigma\mathbf{E}. \qquad (2)$$

Although this equation is true at different scales, is not possible to include all the microscopic conductivity details in models of MEG activity and thus σ refers to macroscopic conductivity with at least 1-mm scale. The division of neuronal currents to primary and volume currents is physiologically meaningful. For example, chemical transmitters in a synapse give rise to primary current mainly inside the postsynaptic cell, whereas the volume current flows passively in the medium, with a distribution depending on the conductivity profile. By finding the primary current we can locate the site of the active brain region.

The primary current is the impetus of both EEG and MEG signals. However, as will be shown later in this section, it is more easy to calculate the magnetic than the electic field due to the symmetries and the particular conductivity distribution of the head. Because EEG electrodes on the scalp or on the cortex are physically in direct contact to the extracellular space, the EEG measures potentials that are associated with the volume currents and driven by the electric field. All currents, both intracellular and extracellular ones, generate magnetic fields. However, as will be shown below, the MEG signals generated in a rather spherical head can be calculated directly from the primary currents without explicit reference to the layered structure of the conductor. Vice versa, solving the inverse problem gives physiologically relevant information on the site, strength, and direction of the intracellular currents at the active brain site.

3. The Current Dipole and Higher-Order Current Multipoles

A current dipole with a dipole moment vector **Q** and position $\mathbf{r}_Q$, approximating a localized primary current, is a widely used concept in neuromagnetism, and can be thought of as concentration of the primary current $\mathbf{J}_p$ to a single point. In MEG (and EEG) applications, a current dipole is used as an equivalent source for the unidirectional primary current that may extend over relatively wide areas of cortex. Most current distributions in the brain are more complex than those produced by a single current dipole. However, any current distribution can be accurately described by a multipole expansion, by adding higher-order terms. In practice, the "dipolarity" of the field patterns depends on *e.g.* the viewing distance because the higher-order terms decrease more rapidly as a function of distance.

4. Solution of Maxwell's Equations: The Forward Problem

Calculation of the external magnetic field from a given current distribution is called the forward problem, and it requires solution of the Maxwell's equations (1) to a reasonable accuracy. All MEG source modelling approaches are based on the comparison of measured data with signals predicted by the model; thus an accurate forward model is a prerequisite for employing a source model. Understanding the properties of a forward model also provides insight to the generation of MEG signals at a more general level. It may be of interest to note that the mathematics underlying MEG analysis can directly (or better: in reverse order) be applied to understanding effects of transcranial magnetic stimulation on the brain.

In the quasistatic approximation, the electric potential V obeys a Poisson equation:

$$\nabla \cdot (\sigma \nabla V) = \nabla \cdot \mathbf{J}_p \tag{3}$$

while the magnetic field is induced by the total current density **J** and is obtained from the Biot-Savart law:

$$\mathbf{B}(\mathbf{r}) = \frac{\mu}{4\pi} \int_G \mathbf{J}(\mathbf{r}') \times \frac{\mathbf{R}}{R^3} dV \tag{4}$$

where the integration is performed over a volume *G* containing all active sources, and $\mathbf{R} = \mathbf{r} - \mathbf{r}'$ is the vector connecting the location of the local source at $\mathbf{r}'$ to point $\mathbf{r}$ where the magnetic field is computed.

It can be shown that in an infinite homogeneous volume conductor the volume currents give no contribution to the electric potential or the magnetic field, which are solely due to the primary currents, $\mathbf{J}_p$. In general, however, a prerequisite for the calculation of the magnetic field is the knowledge of the electric potential distribution, which gives rise to the volume currents according to $\mathbf{J}_v = \sigma \mathbf{E} = -\sigma \nabla V$.

If we assume that the volume where the currents flow consists of homogeneous compartments, the electric potential and magnetic field can be computed from integral equations involving the values of *V* on the surfaces bounding the different compartments (Barnard *et al.,* 1967; Geselowitz 1970). This formulation gives rise to the boundary-element method for calculating the electric and magnetic fields, as discussed below.

B. Neural Current Sources

1. Currents Associated with Action Potentials and Postsynaptic Potentials

Electric signals propagate within the brain along nerve fibers (axons) as a series of action potentials (APs). The corresponding primary current can be approximated by a pair of opposite current dipoles, one at the depolarization and another at the repolarization front (see Fig. 2), and this "quadrupolar" source moves along the axon as the activation propagates. The separation of

the two dipoles depends on the duration of the AP and on the conduction velocity of the fiber. For a cortical axon with a conduction speed of 5 m/s, the opposite dipoles would be about 5 mm apart. Direct magnetic recordings from isolated frog peripheral nerve (Wikswo *et al.,* 1980; Wikswo and van Egeraat 1991) and from intact human peripheral nerves (Erné *et al.,* 1988; Hari *et al.,* 1989) support this simple model.

Insert Figure 2 about here

In synapses, the chemical transmitter molecules change the ion permeabilities of the postsynaptic membrane and a postsynaptic potential (PSP) and current are generated. In contrast to the currents associated with an action potential, the postsynaptic current can be adequately described by a single current dipole oriented along the dendrite. The magnetic field of a current dipole falls off with distance more slowly (in proportion to $1/r^2$) than the field associated with the quadrupolar AP currents (in proportion to $1/r^3$).

Furthermore, temporal summation of currents flowing in neighboring fibers is more effective for synaptic currents, which last up to tens of milliseconds, than for the about 1-ms action potentials. Thus the electromagnetic signals observed outside and on the surface of the head seem to be largely due to the synaptic current flow. In special cases, currents related to action potentials might also significantly contribute to cortical MEG (and EEG) signals, such as, *e.g.,* high-frequency (about 600 Hz) somatosensory responses (Curio *et al.,* 1994; Hashimoto *et al.,* 1996).

The pyramidal cells are the principal type of neurons in the cortex, with their apical dendrites oriented parallel to each other and perpendicular to the cortical surface. Since neurons guide the current flow, the resultant direction of the electrical current flowing in the dendrites is also perpendicular to the cortical sheet of gray matter.

2. Determinants and Estimates of Dipole Strengths

The strength Q of a current dipole associated with postsynaptic currents depends both on the current I and on the length constant λ of the cellular membrane so that $Q = I\lambda$. When more than one neuron is simultaneously active, the total current I depends on the number of cells and synapses activated, on the synchrony of firing, and on the locations of the currents. Considerable cancellation of magnetic fields due to opposite currents and misalignment of fibers takes place in most brain structures.

The length constant λ of the exponential decay is determined by both the conductance of the membrane and the resistance of the intracellular fluid per unit length. It can also be affected by oscillatory background activity (Bernander *et al.,* 1991) and by backpropagating action potentials. Most likely, large cortical cells contribute to the dipole moment relatively more than the small ones because λ increases directly proportional to the diameter of the fiber and because the large cells have more surface area and thereby can obtain more synaptic input.

The magnetic signal per tissue area may increase in some special cases. For example, the spreading depression is associated with strongly enhanced currents due to opening of large ionic channels (Bowyer *et al.,* 1999). In general, calcium- and voltage-sensitive neuronal potassium

currents can largely shape the MEG signals (Wu and Okada 2000), and glial cells (astrocytes), transporting potassium to cerebrospinal fluid, may contribute both as current generators and as amplifiers of synaptic effects. Epileptic discharges are typically associated with strong current densities due to highly synchronous activity. Moreover, the rather unnatural electric stimulation of peripheral nerves triggers a much more synchronized afferent volley than natural tactile stimulation; accordingly, the early cortical somatosensory responses are stronger for electric than tactile stimulation (Forss *et al.,* 1994).

The current I through the synapse can be calculated from the change of voltage during a PSP, and for a single PSP, $Q \approx 20$ fAm. Usually, the current-dipole moments required to explain the evoked magnetic field strengths outside the head are on the order of a few tens of nAm. This would correspond to about a million synapses simultaneously active during a typical evoked response. Since there are approximately 10^5 pyramidal cells per mm^2 of cortex and thousands of synapses per neuron, the simultaneous activation of as few as one synapse in a thousand over an area of one square millimeter would suffice to produce a detectable signal.

However, this type of estimation may not have too much relevance in practice because of considerable cancellation of the generated electromagnetic fields in the misaligned neighboring neurons. According to some estimates, microscopic and translaminar cancellation shadows even 93% of synaptic activity due to spatiotemporal misalignment and asynchronies (Halgren *et al.,* 2000).

Therefore, a better estimate for the activated area might be derived from MEG recordings of guinea pig hippocampal slices which indicate current densities of 4 mA/mm^2, assuming that $\lambda = 0.2\,\mathrm{mm}$ (Okada *et al.,* 1997). Thus a 20-nAm dipole moment would correspond to an about 25 mm^2 area of active cortex. The synchronous elements overshadow the effect of the less synchronous ones in the total signal. For example, it may seem counterintuitive that in a population consisting of 10^7 elements (and thereby corresponding to 1 cm^2 of cortex if one element is equaled to one pyramidal cell) 1% synchronous elements could determine more than 96% of the total signal (Hari *et al.,* 1997). Thus MEG (as well as EEG) sees the most synchronous activity, only.

Although such a synchronous activity may form only a part of the total activity, it can be functionally highly important. For example, invasive recordings from monkey have shown surprisingly large temporal overlap of neuronal firing in many visual cortical areas classically considered as hierarchical processing stages (Schmolesky *et al.,* 1998). Apparently some time markers are required for retaining the temporal order of processing so that the hierarchy will not be violated, and the most synchronous firing could serve such a purpose.

3. Effect of Source Extent

Figure 3 shows that when the activated area is a layer, the dipole is not necessarily located in the center of gravity of the layer but displaced in a characteristical manner. When the layer is extended towards radial direction, the single equivalent current dipole will be more superficial than the center of gravity of the layer, whereas a layer extended in the orthogonal direction will be mislocated to a larger depth.

Insert Figure 3 about here

C. Conductor Models

1. Spherically Symmetric Conductor

If we approximate the head with a layered spherically symmetric conductor ("sphere model"), the magnetic field of a dipole can be derived from a simple analytic expression (Sarvas 1987). An important feature of the sphere model is that the result is independent of the conductivities and thicknesses of the layers; it is sufficient to know the center of symmetry. The calculation of the electric potential is more complicated and requires full information on conductivity (Zhang 1995). Because radial currents do not produce any magnetic field outside a spherically symmetric conductor, MEG is even in realistic conditions to a great extent selectively sensitive to tangential sources. Consequently, EEG data are required for recovering all components of the current distribution. Fig. 4 illustrates these essential properties of MEG.

Insert Figure 4 about here

2. More Realistic Volume Conductor Models

The obvious advantage of a simple forward model is that the field can be computed quickly from a simple analytical formula. The sphere model provides accurate enough estimates for many practical purposes but when the source areas are located deep within the brain or in frontal areas it is necessary to use more accurate approaches (Hämäläinen and Sarvas 1989).

Within a realistic geometry of the head, the Maxwell's equations cannot be solved without numerical techniques. If a boundary-element method (BEM) is applied, electric potential and magnetic field can be calculated numerically starting from integral equations that can be discretized to linear matrix equations (Horacek 1973; Hämäläinen and Sarvas 1989).

In most BEM applications to MEG forward problem, the surfaces are tessellated with triangular elements, assuming either constant or linear variation for the electric potential on each triangle. However, the accuracy of the magnetic-field computation may suffer if a current dipole is located near a triangulated surface. Then some other methods are required to improve the accuracy (Brebbia *et al.,* 1984).

Realistically shaped head geometries of each subject can be extracted from MR images; one example is shown in Fig. 5. The regions of interest, *i.e.*, the brain, the skull and the scalp, are segmented first. The volumes or the surfaces are then discretized for numerical calculations. The segmentation and tessellation problems are still tedious and non-trivial to solve (Dale *et al.,* 1999; Fischl *et al.,* 1999; Lötjönen *et al.,* 1999a; Lötjönen *et al.,* 1999b).

Insert Figure 5 about here

The conductivity of the skull is low, only 1/80 – 1/100 of the brain's conductivity. Therefore most (about 95%) of the current associated with brain activity is limited to the intracranial space,

and a highly accurate model for MEG is obtained by considering only one homogeneous compartment bounded by the skull's inner surface (Hämäläinen and Sarvas 1989; Okada *et al.,* 1999). With suitable image processing techniques it is possible to isolate this surface from high-contrast MRI data with virtually no user intervention. The boundary-element model for EEG is more complex because at least three compartments need to be considered: the scalp, the skull, and the brain.

It is also possible to employ the finite-element method (FEM) or the finite difference method (FDM) in the solution of the forward problem. The solution is then based directly on the discretization of the Poisson's equation governing the electric potential. In this case any three-dimensional conductivity distribution and even anisotropic conductivity can be incorporated (Buchner *et al.,* 1997). However, the solution is more time consuming than with the boundary-element method. Therefore FEM or FDM have not yet been used in routine source modelling algorithms that require repeated calculation of the magnetic field from different source distributions.

III. Instrumentation and Data Acquisition

A. Instruments

1. Field Strengths, SQUIDs, and SQUID Electronics

Figure 6 shows that magnetic signals from the human brain are extremely weak compared with ambient magnetic field variations and also compared with magnetic signals form other parts of the body. Significant magnetic noise is caused, for example, by fluctuations in the earth's geomagnetic field, by moving vehicles and elevators, by radio, television, and microwave transmitters, and by the powerline fields. Thus, rejection of outside disturbances is of utmost importance and is accomplished both by avoiding disturbances near the measurement site, by special magnetic shielding, and by designing the sensors as insensitive as possible to artefacts. Moreover, various noise cancellation techniques can be applied.

Insert Figure 6 about here

The SQUID, the superconducting quantum interference device, is the only detector that offers sufficient sensitivity for the measurement of the tiny magnetic fields (Lounasmaa 1974; Ryhänen *et al.,* 1989). SQUID is a superconducting ring, interrupted by one or two Josephson (1962) junctions. These weak links limit the flow of the supercurrent, which is characterized by the maximum critical current that can be sustained without loss of superconductivity. Dc SQUIDs, with two junctions, are preferred because of lower noise level in rf SQUIDs (Clarke *et al.,* 1976; Tesche *et al.,* 1985). The SQUIDs operate in liquid helium at a temperature of 4 K (-269 C).

If the current through the SQUID is biased to a suitable value, the voltage over the SQUID becomes a periodic function of the magnetic flux threading the ring. Instead of employing a

current bias one can also use voltage biasing whereby the current instead of the voltage over the SQUID is monitored. The period of this characteristic variation is called the flux quantum, $1\Phi_0 = 2.07 \cdot 10^{-15}\mathrm{Wb}$. The SQUID thus acts as an extremely sensitive flux-to-voltage or flux-to-current converter. The voltage over the SQUID is detected with a sensitive amplifier. The response of the electronics is linearized with a feedback circuit, which keeps the output of the SQUID at a constant value.

2. Flux Transformer Configurations

The sensitivity of the SQUID measuring system to external magnetic noise is greatly reduced by the proper design of the flux transformer, a device used for bringing the magnetic signal to the SQUID. Figure 7 shows some flux transformer configurations.

Insert Figure 7 about here

The simplest flux-transformer configuration is the magnetometer which senses the magnetic field with a single coil loop, thus measuring one component of the magnetic field in one location. A magnetometer is also sensitive to homogeneous fields, which are often caused by distant noise sources.

An axial first-order gradiometer consists of a pickup (lower) coil and a compensation coil which are identical in area and connected in series but wound in opposition. This transformer is insensitive to spatially uniform changes in the background field but responds to inhomogeneous changes. Therefore, if the signal of interest arises near the lower coil, it will cause a much greater change of field in the pickup loop than in the more remote compensation coil, thus producing a net change in the output. In effect, the lower loop picks up the signal, while the upper coil compensates for variations in the background field.

Traditionally, most MEG measurements have been performed with axial gradiometers. However, the planar configuration measuring horizontal or off-diagonal gradients of the vertical field component can have advantages over axial coils: the double-D construction (Cohen 1979) is compact in size and it can be fabricated easily with thin-film techniques. The locating accuracies of planar and axial gradiometer arrays are essentially the same for typical superficial sources (Carelli and Leoni 1986; Knuutila *et al.,* 1993). The spatial sensitivity pattern, or "lead field", of off-diagonal gradiometers is narrower and shallower than that of axial gradiometers. These sensors thus collect their signals from a more restricted area near the sources of interest and there is less overlap between lead fields of adjacent sensors in a multichannel array.

Figure 8 shows schematically how the signal distributions picked up by a magnetometer and a planar gradiometer differ. The actual ratio of the maximum signal measured by a planar gradiometer above the source and the peak amplitude of the magnetometer field extrema depends on the depth of the source and the planar gradiometer baseline.

Insert Figure 8 about here

3. State-of-the-Art MEG Systems

The first biomagnetic measurements were performed with single-channel instruments (Cohen 1968; Cohen 1972). However, reliable localization of current sources requires mapping at several locations, which is time-consuming with only one channel. Besides, unique spatial features of, for example, ongoing background neuromagnetic signals cannot be studied. Fortunately, during the last fifteen years multichannel SQUID systems for biomagnetic measurements have developed to reliable commercial products.

A state-of-the art multichannel MEG system comprises more than one hundred channels in a helmet-shaped array to record the magnetic field distribution all around the brain simultaneously. The dewar containing the sensors is attached to a gantry system, which allows easy positioning of the sensors above the subject's head. It is often also possible to move the bed or the chair horizontally.

Figure 9 shows an example of a modern MEG system in use in our laboratory. This Vectorview™ (4D Neuromaging/Neuromag Ltd., Helsinki) device comprises a total of 306 SQUID sensors in 102 three-channel sensor elements, each containing two orthogonal planar gradiometers and one magnetometer. The sensors are arranged into a helmet shaped array, which covers even the most peripheral areas of the brain, such as frontal and temporal lobes and the cerebellum.

Insert Figure 9 about here

In measurements with the modern whole-scalp neuromagnetometers the subject can be either seated or supine. The former orientation is a natural choice in most experiments on healthy subjects while the laying position may be preferred for patients and, of course, for measurements during sleep. In addition to the MEG signals, EEG can be recorded simultaneously with nonmagnetic electrodes and leads.

4. Magnetically Shielded Rooms

For additional rejection of external disturbances, MEG measurements are usually performed in a magnetically shielded room. Four different methods can be employed to construct such an enclosure: ferromagnetic shielding, eddy-current shielding, active compensation, and the recently introduced high-T_c superconducting shielding. Combinations of these techniques have been utlized in many experimental rooms (Cohen 1970; Erné *et al.,* 1981; Kelhä *et al.,* 1982). A typical commercially available room utilized in biomagnetic measurements employs two layers of aluminum and ferromagnetic shielding. The inside floor area is usually 3 by 4 m, and the height is around 2.5 m.

In addition to passive shielding, the exteral disturbances can be also cancelled using active electronic circuits which are either independent of the actual MEG system or integrated with it. The most traditional active compensation system consists of flux-gate magnetometers and pairs of orthogonal Helmholtz coils positioned around the shielded room. The output of the field sensors is employed to control the current fed to the coils to cancel the detected noise.

5. Noise Cancellation in MEG Systems

In addition to the external active shielding, the MEG system may be equipped with compensation sensors, which detect the background signals relatively far away from the head. A suitable proportion of the outputs of the compensation sensors is added to the outputs of the sensors detecting the brain signals. Commercial multichannel MEG instruments using compensation sensors have been pioneered by CTF Systems, Inc. (Port Coquitlam, B.C., Canada). The obvious benefit of this method is that the compensation sensors are almost totally insensitive to brain signals and thus do not affect source identification. On the other hand, the system operation closely depends on the reliability of the noise compensation channels.

It is also possible to compensate noise without employing separate compensation channels. This approach is utilized in the Vectorview system described above. The compensation, performed in the acquisition and analysis software, is based on the signal-space projection (SSP) method (Uusitalo and Ilmoniemi 1997). In this method, the data are processed with a spatial filter, which makes suitable linear combinations of the channels. The filter is tuned to produce zero output if the signal pattern measured by the system is a linear combination of a few characteristic patterns accounting for the noise field found in the shielded room. In the terminology of SSP, these field patterns comprise the *noise subspace* to be removed from the data. This subspace is found by making a recording in an empty room (without subject) and by computing an eigenvalue decomposition of this background noise by principal-component analysis. It turns out that 3 to 8 such component patterns, depending on the environment and the properties of the magnetically shielded room, are required to account for the noise fields.

The benefit of the SSP approach is that separate compensation channels are not needed and that the method does not depend on any single measurement channel being operational. However, since the compensation is based on measurements performed by the sensor array close to the brain, the signal patterns ensuing from the brain may also be modified and thus the filter must be applied to the model data calculated from candidate current sources during data analysis.

B. Data Acquisition and Signal Processing

1. Data Acquisition and Sampling

During data acquisition the analog signals are digitized. The commercial MEG systems are designed to provide amplitude sampling fine enough to fully exploit the dynamic range of the sensors.

The temporal sampling interval determines the highest signal frequency that can be collected undistorted. Sampling a signal with a too low frequency will result in aliasing, *i.e.,* the signal may seem to contain components which are not really there. According to the Nyqvist criterion, the sampling frequency has to be at least twice the highest frequency present in the sampled signal. In practise, the data are typically generously oversampled to show smooth waveforms without additional signal reconstruction procedures and to surpass the nonidealities in the analog antialiasing filters.

In addition to the temporal sampling it is also necessary to provide dense enough spatial sampling of the field to be measured. Since the magnetic field is a vector quantity sampled in a three-dimensional space, a multidimensional generalization of the the Nyqvist criterion has to be applied. It is of interest to note that if several independent measurements, like those made with in the Vectorview system described above, are made at each sampling location, a wider grid spacing can be tolerated without aliasing (Ahonen *et al.,* 1993). The modern whole-head systems provide dense enough spatial sampling of the magnetic field so that the cerebral current sources can be detected without aliasing effects.

In few cases the signal-to-noise ratio (SNR) is sufficient to allow reliable location of current sources without signal averaging: the epileptic discharges and rhythmic background activity have been successfully analyzed from such raw data. When responses to sensory stimuli or voluntary movements are studied one usually resorts to signal averaging. This well-known procedure is based on the assumption that the response of interest is identical after each stimulus and that the noise is additive and uncorrelated across trials. Under these conditions, the SNR improves as $\sqrt{N}$, where N is the number of averaged responses. It turns out that in many evoked responses the signal starts to emerge from noise after just a few averages, obviously indicating that without averaging the SNR is close to one.

2. Signal processing

In many cases, the signal-to-noise ratio for the target phenomena to be studied can be further improved by means of digital signal processing. The most common methods include digital filtering, frequency-domain analysis, coherence and correlation analysis, and spatial filtering. We discuss some essentials of these methods below. Technical treatments of these issues are readily available in textbooks (see, e.g., Jenkins and Watts 1968; Oppenheim and Schafer 1975).

It is customary to collect the data with a relatively wide bandwidth to allow selection of the desired final bandpass in postprocessing. In evoked response studies, the averaged signals are often lowpass filtered digitally to suppress high-frequency noise. If most of the signal energy in spontaneous MEG activity is concentrated to a relatively narrow bandwidth, after bandpass filtering the signal-to-noise ratio may be high enough for source analysis of the unaveraged rhythmic activity.

A time-dependent signal can be presented equivalently in time and frequency domains. However, the Fourier spectra can often reveal some characteristics not easily recognizable in the time-domain analysis. A sophisticated frequency analysis may aim at identifying short-time changes in narrowband rhytmic activity, which requires the calculation of spectrograms and sometimes their averaging time locked to a stimulus. Such calculations can also be performed by employing wavelet transforms (see, e.g., Schiff *et al.,* 1994; Quiroga and Schürmann 1999). More straigthforward analyses have been performed by taking an absolute value (Salmelin and Hari 1994) or square (Pfurtscheller and Aranibar 1977; Pfurtscheller 1992) of the band-pass filtered spontaneous activity and then averaging the data time-locked to a stimulus, movement, or other event. As a result one can follow the level of the rhythmic activity on the desired frequency band as a function of time, and the activity contributing to the result doesn't need to be time-locked to the triggering event. This approach has been applied in both EEG (Pfurtscheller and Aranibar

1977) and MEG (Salmelin and Hari 1994; Salmelin *et al*., 1995) studies on the temporospatial reactivity of the sensorimotor mu rhythm in relationship to voluntary movements(Salmelin and Hari 1994; Salmelin *et al*., 1995).

Cooperative behavior of several brain regions can be studied by calculating cross-correlations or coherence spectra across different signal channels. As described in section III.A.2, the planar gradiometers employed in some neuromagnetometers are sensitive to currents in the vicinity of each sensor. Therefore, calculation of correlations and coherence between planar gradiometer channels gives useful information about the characteriscs of the underlying regions in the brain. Correlation and coherence analysis can be also extended to virtual channels, specifically tuned to detect activity of desired brain areas (Gross *et al.,* 2001).

The rationale for using *spatial* filters instead of traditional filtering in time domain is based on the assumption that the signal of interest has a distribution different from the environmental noise, biological artefacts, or uninteresting brain activity. In section III.A.5. we already discussed one particular spatial filter, the signal-space projection method. It is evident that the noise subspace to be removed from the data may contain field patterns of, for example, cardiac artefacts, whose contribution can thus be removed, or at least suppressed, by applying a projection operator.

3. Monitoring the Head Position During a Measurement

To obtain the position of the subject's head, an anatomical head-based coordinate system has to be related to a device coordinate system fixed to the MEG sensor array. To this end, three or more small coils can be attached on the surface of the head and their locations can be measured in relation to anatomical landmarks, such as nasion and preauricular points. During the MEG acquisition, excitation currents are fed to the coils and the produced magnetic field is measured (Knuutila *et al.,* 1985; Erné *et al.,* 1987).

The locations of the indicator coils can then be determined by modelling them as magnetic dipoles, *i.e.*, small current loops, and by iteratively adjusting the coil locations and orientations until the best match between the measured signals and those predicted from the coils is achieved. Since the coil locations are thus known both in the device and anatomical coordinate systems, their relative locations and orientations can be determined. The head position is measured routinely in the beginning, and sometimes also at the end of each recording, to ensure stable head position.

This routine procedure requires that the subject keeps her head still during the measurements which may be difficult even for cooperative subjects when the measurement is long or when the subject has a motor task. Individual bite bars can be used to avoid head movements (Singh *et al.,* 1997), but some subjects find them rather uncomfortable; biting may also cause muscle artifacts. Furthermore, bite bars cannot be applied in experiments requiring verbal responses.

Because of head movements, the locations of the inferred current sources are offset from their true values or the results of applying distributed source estimation methods may be blurred more than in the case of an acquisition with a cooperative subject.

Fast methods are being developed to measure head position continuously or intermittently during the whole recording. To speed up the measurement, the coils on the scalp can be activated simultaneously with different temporal patterns. Since the magnetic field is linearly related to the current fed to the coils, the magnetic fields produced by individual coils can be extracted from the measured signal components.

The continuous records of the head movements can then be utilized in different correction methods. If the signal-to-noise ratio is so good that unaveraged signals can be modeled, one can simply use a different coordinate transformation between the anatomical and device coordinate frames at each time instant. The situation is more complicated if signals are averaged or if continuous data segments containing signals from supposedly identical source distributions are compared. Uutela et al. (2001) have recently explored several alternative computational approaches applicable to signal averaging and source modelling in situations with significant head movements during the data acquisition.

C. Artifacts in MEG Recordings

Magnetic artifacts due to fluctuations in the earth's magnetic field, moving vehicles, radio transmitters, or power lines are effectively attenuated in a magnetically shielded room. Noise can also be reduced by higher order gradiometers, but the accompanying decrease in sensitivity, and difficulties in interpreting the data, discourage this approach. Even within a magnetically shielded environment, disturbances can arise, for example, from stimulators and monitoring devices containing moving magnetic materials. Figure 10 shows some typical MEG artefacts.

Insert Figure 10 about here

1. Eye Blinks and Eye Movements

Eye movements and blinks are important biological sources of MEG artifacts. Blinks may be time-locked to the stimuli, especially if the stimuli are strong and alerting, and the signals can be of the order of 3 – 4 pT above the lateral aspects of the orbits (Antervo *et al.,* 1985). The corneo-retinal potential is the ”battery” of both the blink and the eye-movement signals but the generation mechanisms differ. The blink signals are caused by changes in the volume conductor geometry whereas during eye movements the orientation of the source currents changes in reference to the volume conductor. Because of the large amplitude of these eye-related artifacts, it is recommended to monitor the electro-oculogram during all MEG recordings to be able to reject epochs coinciding with blinks and eye movements.

2. Cardiac Artifacts

Both magnetocardiogram(MCG)-related and ballistocardiogram-related artifacts may be associated with the cardiac cycle. Jousmäki and Hari (1996) have shown that the cardiac-related MEG artefacts are produced by the electric activity of the heart (MCG) whereas the blood-flow related susceptibility artifacts are negligible in healthy subjects. The MCG contamination, typically evident as the R peak, is stronger in the left than right-hemisphere MEG channels and

depends on the position of the heart with respect to the head. In children, the shorter heart-brain distance may cause more MCG-related artifacts.

3. Other Artifacts

Artefacts may also arise *e.g.* from respiration if the clothing or the body of the subject contain some magnetic material. Muscle contractions in the neck and face areas can also produce artefacts. However, muscular contamination seems to be weaker in MEG than EEG measurements, probably because the distance to the sources of the muscle artifacts is significantly larger for MEG sensors than for EEG electrodes.

4. Elimination of Artifacts

Prevention is always the best way to deal with artifacts and it often works for external magnetic noise, stimulation-related artefacts, etc. It is also possible to reject all traces coinciding with some biological artifacts, such as eye blink and eye movement related signals. The procedure typically works well but can bias the results in some experiments because certain states of the subject are not included to the analysis.

It is also possible to analyse only signals which follow/or precede a known artefact by a fixed time; for example, the analysis can be "gated" by the simultaneously recorded ECG and its large QRS complex (Murayama *et al*., 2001).

Finally, if artifacts cannot be avoided, their influence on the signals should be minimized. The signal-space projection method may largely suppress some artefacts but the method should be applied with caution when the exact noise pattern and the signal patterns are not known in advance.

IV. Source Analysis

A. The Inverse Problem

The goal of the neuromagnetic inverse problem is to estimate the source current density underlying the MEG signals measured outside the head. Unfortunately, the primary current distribution cannot be recovered uniquely, even if the the magnetic field (or the electric potential) were precisely known everywhere outside the head (Helmholtz 1953). However, it is often possible to use additional physiological information to constrain the problem and to facilitate the solution. One approach is to replace the actual current sources by equivalent generators that are characterized by a few parameters. A unique solution for the parameters may then be obtained from the measured data by, *e.g.,* a least-squares-fit. Thus the solution of the forward problem is a prerequisite for most localization studies.

Figure 11 illustrates ambiguities encountered in the solution of the inverse problem. In this simulation, the data were calculated from a single current dipole in the right auditory cortex. When the current dipole model is applied, the correct solution is, naturally, obtained. However,

when these same data are analyzed with the minimum-norm estimate (MNE), the result is a smooth, widespread current distribution, because that gives rise to exactly the same field distribution as the current dipole. Vice versa, when a widespread current distribution is analyzed, the result of dipole modelling is, erroneously, a very local source whereas the MNE approach gives the correct answer. It is thus evident that the result of the analysis depends crucially on the underlying assumptions of the source modelling method.

Insert Figure 11 about here

B. Statistical Framework: The Bayesian Approach

Most source modelling approaches can be conveniently described within the Bayesian statistical framework ("the statistical inversion theory") (Tarantola 1987). In this approach physical quantities are modelled as random variables with associated probability distributions. The solution of the inverse problem is then a probability distribution, conditioned on the observation. The estimates for the interesting (target) quantities are calculated from the measurement data on the basis of this conditional "a posteriori" distribution.

If the observable quantities contained in the measured data are arranged into a vector **y** and the unknowns into **x**, respectively, the Bayes' theorem states:

$$f_{post}(\mathbf{x}) = C\, f_{prior}(\mathbf{x}) f(\mathbf{y} \mid \mathbf{x}) \qquad (4)$$

where $f_{post}(\mathbf{x})$ is the a posteriori probability distribution of the unknown quantities, C is a constant, $f_{prior}(\mathbf{x})$ is the a priori distribution reflecting the a priori information we want to employ in the modelling, and $f(\mathbf{y} \mid \mathbf{x})$ is the distribution of the measured data, in the presense of noise, assuming that the target quantities have the values given in **x**. In MEG analysis, **y** consists of the measured magnetic field values as a function of time and **x** contains the unknown parameters of our current distribution model.

If the noise is assumed to be Gaussian, the Bayesian approach leads to standard least-squares fitting method, which actually provides the set of parameters maximizing $f_{post}(\mathbf{x})$ also called the maximum a posteriori estimate (MAP). In addition to the MAP estimate it is customary to calculate confidence limits for the unknown parameters **x** which describe the 'width' of $f_{post}(\mathbf{x})$ around the maximum.

The benefit of resorting to the statistical inversion theory as the initial step of source analysis is that the basic problem of selecting an appropriate model is clearly separated from the technical problems of calculating desired characteristics of $f_{post}(\mathbf{x})$. Furthermore, a priori assumptions, such as anatomical or functional constraints obtained from MRI, fMRI, or PET can be incorporated in a natural fashion. It should be emphasized, though, that computational cost for providing other properties of $f_{post}(\mathbf{x})$ than the MAP estimate can be prohibitive. These properties include, in particular, marginal distributions, which are often needed to visualize $f_{post}(\mathbf{x})$, which is a function of multiple variables. There have been attempts to employ the statistical inversion

theory directly to calculate, *e.g.,* a posteriori probablities of several candidate current source models directly from $f_{post}(\mathbf{x})$ (Schmidt *et al.,* 1999).

C. Parametric Source Models

1. The Current Dipole Model

The simplest physiologically sound model for the neural current distribution consists of one or more point sources, current dipoles. In the simplest case the field distribution measured at one time instant is modelled by that produced by one current dipole (Tuomisto *et al.,* 1983). The best-fitting current dipole, commonly called the equivalent current dipole (ECD), can be found reliably by using standard non-linear least-squares optimization methods, ((see, e.g., Marquardt 1963)). Some authors have successfully used "dipole density plots", the number of dipoles per unit area, to quantify the strength of activation of a certain brain region (Vieth *et al.,* 1996; Amidzic *et al.,* 2001).

If the same experiment is repeated several times, the locations of the dipoles as well as their amplitudes and orientations will be different because of instrumental noise and ongoing background activity. Therefore, it is useful to compute the dipole parameter confidence in addition to the best-fitting parameters (Hämäläinen *et al.,* 1993).

In the time-varying dipole model, first introduced to the analysis of EEG data (Scherg and von Cramon 1985; Scherg 1990), an epoch of data is modeled with a set of current dipoles whose orientations and locations are fixed but the amplitudes are allowed to vary with time. This approach corresponds to the idea of small patches of the cerebral cortex or other structures activated simultaneously or in a sequence. The precise details of the current distribution within each patch cannot be revealed by the measurements, performed at a distance in excess of 3 cm from the sources.

If we arrange the epoch of data into a matrix **B** whose columns contain the measured signals at each time instant, a time-varying multidipole model, consisting of p dipoles, can be written as

$$\mathbf{B} = \mathbf{G}(\mathbf{r}_1,\ldots,\mathbf{r}_p,\hat{\mathbf{e}}_1,\ldots\hat{\mathbf{e}}_p)\mathbf{Q} + \mathbf{N}\,, \tag{5}$$

where **G** is a gain matrix relating the dipole amplitudes to the measurements, **Q** is a matrix whose rows, $\mathbf{q}_1^T \ldots \mathbf{q}_p^T$, contain the temporal waveforms of the dipoles, and **N** is a matrix of noise with a Gaussian distribution, independent across different time points, with a known time-independent covariance matrix. The columns of **G**, $\mathbf{g}_1(\mathbf{r}_1,\hat{\mathbf{e}}_1)\ldots\mathbf{g}_p(\mathbf{r}_p,\hat{\mathbf{e}}_p)$, are the field distributions generated by dipoles located at $\mathbf{r}_1,\ldots,\mathbf{r}_p$ with orientations by $\hat{\mathbf{e}}_1,\ldots\hat{\mathbf{e}}_p$. The idea of the model is schematically depicted in Fig. 12.

Insert Figure 12 about here.

It is evident that an important initial step in dipole modelling is the selection of the number of sources, *p*. This selection can be based on the singular-value decomposition of the data matrix **B**.

Ideally, the singular values should first decrease gradually, followed by a plateau corresponding to the additive noise, **N**. In practice, however, such a separation may be far from trivial. One possibility to handle this problem is to build the source model gradually and to require that each new dipole introduced clearly explains some temporal or spatial aspects of the data. In the MUSIC approach described in the next section, the separation of the 'noise subspace' corresponding to **N** is not very critical and the model order can be actually rather safely somewhat overestimated without causing a misinterpretation.

As a result of the modelling one obtains the orientations and locations of the dipoles, as well as the temporal evolutions of the sources strengths. Again, the optimal source parameters are found by matching the measured data collected over a period of time with those predicted by the model using the least-squares criterion.

From a mathematical point of view, finding the best-fitting parameters for the time-varying multidipole model is a challenging task. Since the measured fields depend nonlinearly on the dipole position parameters, standard least-squares minimization routines may not yield the globally optimal estimates for these parameters. Therefore, more complex optimization algorithms (Uutela *et al.,* 1998; Aine *et al.,* 2000; Huang *et al.,* 2000) and special fitting strategies (Berg and Scherg 1996) have been suggested to take into account the physiological characteristics related to particular experiments. For each set of dipole position and orientation candidates it is, however, straightforward to calculate the optimal source strength waveforms using linear least-squares optimization methods (see, e.g., Mosher *et al.,* 1992).

Even with advanced numerical methods, the optimization problem of the time-varying dipole model may not be solved adequately. First, there might be competing solutions with different source configurations but indiscernible from each other in the presense of measurement noise. Second, the actual source distribution may not be well approximated by a dipole. Therefore, manually guided fitting strategies are often employed. It is then possible to include 'fuzzy' prior information and to build the model gradually in a bottom-up fashion. One can identify the first source at a time when the field pattern reliably suggests a single source or several sources far apart. For example, the primary somatosensory cortex SI can be identified at an earlier time point than the second somatosensory cortex SII after a stimulus to a peripheral nerve (Hari *et al.,* 1993b). When necessary, the effects of known (previously identified) sources can be removed before identifying a new source. The complete model consists of several dipoles with time-varying strengths. An important final step in the model construction is to compare waveforms predicted by the model with the measured signals.

2. MUSIC Approaches

As discussed above, finding the locations of multiple current dipoles is a complex task. If non-dipolar sources are present it may be difficult to find the correct solution even if the minimization algorithm would perform optimally for dipoles. Therefore, a less restricted correlation technique known as multiple signal characterization (MUSIC) (Schmidt 1986) has been introduced for MEG and EEG analysis (Mosher *et al.,* 1992).

The primary assumption in MUSIC approaches is that the time series of the dipoles in Eq. (5) are linearly independent. More recently the method has been extended to synchronous sources

(Mosher and Leahy 1998) and to nondipolar sources (Mosher *et al.,* 1999), corresponding to the higher-order terms of the current multipole expansion (Katila 1983).

The benefit of the MUSIC approach over the traditional least-squares search is that the optimization problem is replaced by searching peaks in a scalar correlation measure calculated over a three-dimensional grid covering the viable dipole locations. In the original 'classical' MUSIC appoach several local maxima had to be identified at once. The more sophisticated RAP-MUSIC (Recursively Applied and Projected MUSIC) algorithm (Mosher and Leahy 1999) employs the signal-space projection approach to remove the contributions of the dipoles already identified so that it is sufficient to find the global maximum of the correlation cost function at each iteration of the algorithm.

The RAP-MUSIC algorithm is likely to perform better than a traditional multidipole search in the presence of distributed, non-dipolar sources. RAP-MUSIC is also computationally effective and allows the model to be constructed one source at a time.

3. Verification of Dipole Models

The rather complex multidipole models should in many cases be constructed from bottom to up, starting from sources/areas which are already known to be activated by the stimuli used in the study, and then explain the remaining parts of the signals as carefully as possible. It is also important to pay attention to the consistency of the solutions, both within and across subjects. Other types of verification can be obtained by studying patients who have lesions in the assumed source areas or by recording electric signals during surgery. For example, the SII sources first detected by MEG have been later confirmed by intraoperative recordings, which have displayed very similar waveforms from the assumed source areas (Allison *et al.,* 1989).

D. Current Distribution Models

An alternative approach in source modelling is to assume that the sources are distributed within a volume or surface, often called the source space, and then to use various estimation techniques to find out the most plausible source distribution. The source space may be a volume defined by the brain or restricted to the cerebral cortex, determined from MR images. These techniques may provide reasonable estimates of complex source configurations without having to resort to complicated dipole fitting strategies. However, even when the actual source is pointlike, its image is typically blurred and can have an extent of a few cm in each linear dimension, depending on the method employed (see Fig. 11) Therefore, the size of an activated region in the source images need not relate to the actual dimensions of the source but rather reflects an intrinsic limitation of the imaging method. In fact, without an extremely high signal-to-noise ratio it is unrealistic to claim that it would be possible to determine the extent of a source giving rise to the MEG signals (Nolte and Curio 2000).

1. Linear Minimum-Norm Solutions

The first current-distribution model applied in MEG analysis was the (unweighted) minimum-norm estimate (Hämäläinen and Ilmoniemi 1984; 1994), one in a group of linear

approaches which can be described in a common framework. Here linearity means that the amplitudes of the currents are obtained by multiplying the data with a (time-independent) matrix. This kind of estimates have been employed by several authors (see, e.g. Dale and Sereno 1993; Fuchs *et al.,* 1999).

In Bayesian framework, the measurements are modelled with a distribution of current dipoles whose amplitudes have a Gaussian distribution with a known covariance matrix $\mathbf{C}_q$. The measurements contain noise which is Gaussian with a known covariance matrix $\mathbf{C}_b$. It is common to use a discrete grid of current locations even though a continuous formulation is also possible (Ioannides *et al.,* 1990; Hämäläinen and Ilmoniemi 1994). In the discrete approach, the MAP estimate for the current distribution is obtained from

$$\mathbf{q}_{\mathrm{MAP}} = \arg\min_{\mathbf{q}} \left\{ (\mathbf{b} - \mathbf{G}\mathbf{q})^T \mathbf{C}_b^{-1} (\mathbf{b} - \mathbf{G}\mathbf{q}) + \mathbf{q}^T \mathbf{C}_q^{-1} \mathbf{q} \right\}, \tag{6}$$

where $\mathbf{q}$ is a vector of the dipole strengths, $\mathbf{G}$ is, as before, the solution of the forward problem, *i.e.*, the gain matrix relating the measured signals $\mathbf{b}$ to the dipole strengths, the superscript T denotes the matrix transpose, and arg min indicates the value at which the function inside the braces is minimized. The first term indicates the difference between the measured data and those predicted by the model, $\mathbf{G}\mathbf{q}$. The second term is the (weighted) size of the current distribution. These estimates are sometimes also called L2-norm solutions because of the quadratic cost function (second term in Eq. (6)) associated with the Gaussian probability distribution assumed for the source strengths. Computationally, this approach has the benefit that the solution is linear:

$$\mathbf{q}_{MAP} = \mathbf{C}_q \mathbf{G}^T (\mathbf{G}\mathbf{C}_q \mathbf{G}^T + \mathbf{C}_b)^{-1} \mathbf{b}. \tag{7}$$

In the original minimum-norm approach $\mathbf{C}_q = s^2 \mathbf{I}$, where $\mathbf{I}$ is an identity matrix and s^2 is the expected variance of the source strength. If $s^2 \to 0$, the estimate vanishes whereas in the limit $s^2 \to \infty$ we have

$$\mathbf{q}_{MAP} = \mathbf{G}^T (\mathbf{G}\mathbf{G}^T)^{-1} \mathbf{b}. \tag{8}$$

Since the sources are typically close to each other in the source space, some columns of $\mathbf{G}$, *i.e.*, the field distributions of different currents may be almost similar and the matrix to be inverted above in Eq. (8) is ill-conditioned. Thus, small errors in $\mathbf{b}$ are magnified and unrealistically large complicated current patterns may appear. According to Eq. (7), the assumption of a finite variance leads to adding a second term inside the matrix inversion which serves to regularize the problem, *i.e.*, to suppress spurious high-amplitude solutions. When s decreases, the contribution of the second term becomes more significant and larger errors between the measured and predicted data are thus accepted to avoid explaining the noise. Selection of a reasonable value for the (unknown) variance s^2 thus becomes important.

Several methods can be used to cope with this regularization problem. One possibility is to estimate the signal-to-noise ratio from the data and to use it to define a proper value for the source variance (Dale *et al.,* 2000). Another approach is to consider the relative sizes of the two

terms in Eq. (6). The L-curve method (Hansen 1992) makes this consideration formal by plotting the two terms against each other and by selecting an inflection point where the rapid decrease of the source power stops and the error in data explanation sets off.

If an equal source variance is assumed throughout the source volume, the MNE is biased towards superficial currents. Because the total current necessary to explain the data is smaller if the current elements are closer to the sensors. There have been several attempts to avoid this undesirable tendency. First, the expected source variance can be made depth-dependent. The most popular choice is a lead-field weighting, *i.e.*, $R_{kk} = \beta / \mathbf{g}_k^T \mathbf{g}_k$, where R_{kk} is the variance of the *k*th source and $\mathbf{g}_k$ is the *k*th column of $\mathbf{G}$ (Deeper currents are thus expected to be stronger to compensate the signal fall-off as a function of distance. Another possibility is to restrict the source space to currents normal to the cortex by using high-resolution MRI information (Dale and Sereno 1993). This method seems to improve the depth bias to some extent but is not entirely satisfactory either. Finally, it is possible to adjust the expected source variance as a function of source location on the basis of supplementary imaging, *e.g.*, fMRI information.

In addition to the depth bias, the MNEs fail to truthfully reflect the actual extent of the underlying current sources. Simulations have shown that the point spread of the estimate, *i.e.*, the image of a focal current source is a function of the source location (Dale *et al.,* 2000). In addition, the spread depends on the assumed source variance. Thus, any inferences about the size of the estimated areas from MNEs have to be dealt with extreme caution. It is evident that the dipole estimates share a similar problem: the source is always focal even if the true distribution is diffuse (see Fig. 11). In dipole analysis, however, one is usually well aware of this deficiency and thus dipoles are always considered to approximate the activation of a finite-sized patch of cortex. In both cases novice users of MEG may be easily misled when the sources are represented in a visually suggestive and attractive fashion in context with the underlying anatomy obtained from MRI.

Recently, attempts have been made to defeat the problems associated with true *vs*. estimated source extent by presenting statistical parametric maps (SPM) instead of MAP estimates (Dale *et al.,* 2000). These maps present spatial distributions of statistical test variables, which can be used to assign confidence levels in hypothesis testing. For example, by dividing the scalar current strength in the MAP estimate by its variance (Dale *et al.,* 2000) one obtains a test variable to find locations where the estimated current value is significantly different from zero. It turns out that the point-spread functions vary less as a function of source location in the SPMs than in the MAP estimates. However, the strength of a source with fixed extent can vary considerably depending on the synchrony and amount of synaptic activity. Thus it would be highly misleading to trust the source extent estimate of the SPM algorithm under such conditions: apparent changes in the extension of the source area could just reflect changes of the source strength because stronger signals differ statistically significantly from zero over a wider area.

It is also possible to extend the minimum-norm approach to source covariance matrices with non-zero off-diagonal elements. This choice makes currents in different, typically neighbouring, nodes of the reconstruction grid behave in an orderly fashion. One particular approach is to define $\mathbf{C}_q$ as the inverse of a discrete spatial Laplacian operator. According to Eq. (6) this means that smooth currents with a smaller Laplacian are preferred. This method, called LORETA (LOw

Resolution Electromagnetic TomogrAphy) (Pascual-Marqui *et al.,* 1995) seems to provide smaller mislocalization as measured by the the peak of the current estimate than the linear estimates employing a diagonal $\mathbf{C}_q$ (Fuchs *et al.,* 1999). However, the pointspread functions are wider, *i.e.*, the current estimates are even more blurred than those obtained without the Laplacian constraint.

As an example of a sophisticated application of the minimum-norm estimates, Fig. 13 shows data from a recent paper by Dale *et al.* (2000). These authors employed a cortically-constrained source space and presented the current estimates in an anatomical display where the cortical mantle was inflated to open up the sulci.

Insert Figure 13 about here

2. Minimum-Current Estimates

It is also possible to enter into the source imaging method the assumption that the activated areas have a small spatial extent. For example, the MFT (Magnetic Field Tomography) algorithm obtains the solution as a result of an iteration in which the probability weighting is based on the previous current estimate (Ioannides *et al.,* 1990). Another possibility is to use a probability weighting derived from the MUSIC algorithm, combined with cortical constraints (Dale and Sereno 1993).

The l1-norm approach employs the sum of the absolute values of the current over the source space as the criterion to select the best current distribution among those compatible with the measurement (Matsuura and Okabe 1997, , 1995 #1245; Uutela *et al.,* 1999). The amplitudes of the currents are assumed to have a exponential instead of a Gaussian distribution. The MAP estimate is then obtained from

$$\mathbf{q}_{\mathrm{MAP}} = \arg\min_{\mathbf{q}} \left\{ (\mathbf{b} - \mathbf{G}\mathbf{q})^T \mathbf{C}_b^{-1} (\mathbf{b} - \mathbf{G}\mathbf{q}) + \sum_k |q_k| \right\}, \qquad (9)$$

where $|q_k|$ is the absolute value of the current at the kth location of the source space. In contrast to the traditional l2-norm cost function, Eq. (6), the l1-norm criterion yields estimates focused to a few small areas within the source space. However, the result of the minimization cannot be any more expressed in a closed form. The l1-norm solutions are sometimes referred to as minimum-current estimates (MCEs) to distinguish them from the l2-norm MNEs.

Figure 14 shows an example of the MCEs in normal-hearing subjects who were viewing sign language (Levänen *et al.,* 2001). The MCEs are from individual left hemispheres at different times after the onset of the sign and illustrate activations in the inferior frontal lobe (IFL), the superior temporl sulcus (STS), and in the visual motion-sensitive area V5.

Insert Figure 14 about here

V. Neuromagnetic Studies

This section briefly discusses examples of neuromagnetic studies, selected to portray how the data analysis methods described in the previous sections are employed in practise. The examples also demonstrate the importance of using a suitable experimental paradigm to facilitate the data analysis and interpretation.

1. Sequence of Evoked Responses

Our first example illustrates the analysis and interpretation of evoked responses to simple somatosensory stimuli; for more details about the characterization of somatosensory evoked magnetic fields, see, *e.g.,* Hari and Forss (1999). Figure 15 shows a typical evoked response distribution to stimulation of the right median nerve; 124 responses were averaged at all 204 gradiometers of the whole-scalp neuromagnetometer. The main responses peak around 21 ms over the contralateral primary somatosensory cortex SI and later, around 100 ms, over both SII areas at the lateral aspects of the hemispheres. Source analysis with a 3-dipole model (see Figure 16) showed activation first at the left SI hand area and later in the SII cortices of both hemispheres.

The easy distinction between signals from the various somatosensory cortices by MEG recordings allows monitoring of activity changes in association with different tasks and types of sensory inputs, and it has also turned out to be clinically useful in studies of different patient groups. For example, patients with Unverrrich–Lundborg type progressive myoclonus epilepsy show strongly enhanced responses at SI, facilitated callosal tansfer to the ipsilateral SI, and absent SII responses (Forss *et al.,* 2001).

Insert Figures 15 and 16 about here

2. Cortex-Muscle Coherence

The spontaneous electric activity of the human brain consists of several rhythmic components, many of which have a characteristic spatial distribution. For example, the primary sensorimotor cortices generate “mu rhythm” which consists of prominent frequencies around 10 and 20 Hz (Hari and Salmelin 1997). The 20-Hz activity is prominent in the primary motor cortex and, consequently, changes of its level have been utilized as indicators of the functional state of the motor cortex (Schnitzler *et al.,* 1995; Hari *et al.,* 1998).

As an example of the analysis of ongoing spontaneous activity we present some results from the studies on the 20-Hz activity of the motor cortex. These signals are coherent with surface electromyogram during isometric contraction (Conway *et al.,* 1995; Salenius *et al.,* 1997a), reflecting rhythmic drive from the motor cortex to the spinal motor neuron pool. Figure 17 shows that both the EMG signal from an isometrically contracted foot muscle and the simultaneously recorded MEG from the rolandic region are rhythmic but their waveshapes differ. The coherence spectra, also shown in Fig. 17, were calculated between the MEG and EMG signals. They were clearly above the noise level around 20 Hz, both for hand and foot muscles, suggesting that the cortex and muscle speak to each other at these frequencies (Salenius *et al.,* 1997b). The coherent cortical activity shows a gross somatotopical organization: the maxima of the coherent MEG

signals occur laterally along the central sulcus during upper limb contractions and close to the brain midline during lower limb contractions. For trunk muscles, the motor representation, revealed by means of cortex–muscle coherence, is in-between the foot and hand muscle representations (Murayama *et al.,* 2001). The coherence between cortex and trunk muscles is technically rather difficult to measure because the signals are small and the surface EMG is easily contaminated by electrocardiographic signals; therefore analysis time-locked to the R-peaks of the ECG had to be applied (Murayama *et al*., 2001).

Insert Figure 16 about here

It is interesting that the MEG signal precedes the EMG with a time lag that systematically increases with the conduction distance from cortex to muscle. Similar results have been obtained from calculations based on cross-correlograms that show phase lags between the MEG and EMG signals, from phase-spectra that show linearities at some frequency ranges, and from MEG signals back-averaged from the EMG onsets (Salenius *et al.,* 1997b; Brown *et al.,* 1998; Gross *et al.,* 2000). The delays between MEG and EMG signals, computed from their phase differences at the best cortex–muscle synchrony, were in excellent agreement with conduction times from the motor cortex to the respective muscle observed in transcranial magnetic stimulation studies (Gross *et al.,* 2000).

The cortex–muscle coherence can also be also used as a tool for identifying the primary motor cortex, and we have routinely applied the MEG–EMG coherence in presurgical evaluation of patients with tumor or epilepsy for such purposes (Mäkelä *et al.,* 2001).

3. Dynamics of the Human Mirror-Neuron System

Humans copy other persons' actions during the whole life, most of the time automatically and effortlessly. Practioners of sports also know that viewing another person's movements facilitates own motor models. This automatic imitation behavior is most likely supported by the mirror-neuron system that was first identified and characterized in the monkey premotor cortical area F5 (Rizzolatti *et al.,* 1996a). This area contains "mirror neurons" that discharge both when a monkey executes hand actions and when he observes the same actions made by another monkey or by the experimenter. The mirror-neuron system matches action observation and execution, and it may play an important role both in action imitation and in understanding the meaning of actions made by other subjects, thereby also having relevance for social interactions.

Several recent brain imaging studies clearly demonstrate the existence of a mirror-neuron system also in the human brain (Fadiga *et al.,* 1995; Rizzolatti *et al.,* 1996b; Hari *et al.,* 1998; Iacoboni *et al.,* 1999; Nishitani and Hari 2000a; Strafella and Paus 2000).

Nishtani and Hari (2000a) aimed at identifying the temporal dynamics of the cortical activation sequence within the human mirror neuron system. They employed a four-dipole model to explain the measured data. Figure 18 shows that when the subjects performed, observed, or imitated right-hand reaching movements which ended with a precision pinch of the top of a manipulandum, activations were found in the left occipital visual cortex, the left posterior inferior frontal area (Broca's area) and the primary motor cortices bilaterally. All these areas are thus involved in the human mirror neuron system.

Insert Figure 18 about here

During execution, the left Broca's area was activated first (peak ~250 ms before the pinching). This was followed within 100–200 ms by activation in the left primary motor cortex, and 150–250 ms later in the right motor cortex. The relative timing of the cortical activation sequence from Broca's area to the left and finally to the right motor cortex was similar also during imitation and observation. However, both Broca's area and motor cortex were activated about twice as strongly during on-line imitation than during self-paced execution and passive observation. Thus both timing and source strength data suggest that the Broca's region, the human counterpart of the monkey mirror neuron area F5, plays a key role in the human mirror-neuron system.

More recent studies using photographs of lip forms as stimuli (Nishitani and Hari 2000b) have shown that activation of Broca's area is often preceded by signals generated in the region of the superior temporal sulcus. The human mirror-neuron system includes at least the STS region, Broca's area, the primary motor cortex, the superior parietal lobe, and the somatosensory cortices.

4. Binaural Hearing Studied in Frequency Domain

In normal hearing, sounds activate our brains through two ears, and the inputs from each ear reach the auditory cortices of both hemispheres (Fig. 19, top). The resulting binaural cortical responses are thus a mixture of inputs from both ears and it has not been possible to find out which part of responses to binaural sounds derives from either ear. Fujiki et al. (2001) solved this problem by labeling the auditory inputs from both ears by "frequency-tags": Continuous 1-kHz tones, presented either monaurally to left or right ear, or binaurally were amplitude modulated (left-ear tone at 26.1 Hz and the right-ear tone at 20.1 Hz). An analogous frequency tagging has been previously used to study visual binocular interactions (Brown *et al.,* 1999)and to label different melodies with amplitude modulations (Patel and Balaban 2000).

Figure 19 shows analysis of the resulting MEG signals in frequency domain. In the left hemisphere, responses to ipsilateral sounds were significantly suppressed during binaural presentation, whereas responses to contralateral tones were not significantly affected. The left hemisphere's preference to right-ear input was accentuated during binaural hearing, possibly providing the neuronal basis for the well-known "right-ear advantage" in right-handed subjects during dichotic listening. In the right hemisphere, the responses were significantly and similarly suppressed for both contralateral and ipsilateral sounds. This noninvasive analysis of contributions of the two ears to binaural cortical responses indicates that the inputs from the two ears compete strongly in the human auditory cortex but with clear hemispheric differences.

Insert Figure 19 about here

5. Preoperative Functional Localization

MEG has been suceesfully used in preoperative identification of the somatomotor strip in patients with brain tumors and epilepsy. Figure 20 shows one such example. The functional

landmarks used to identify central sulcus were based on somatosensory responses to hand, foot, and lip stimulation that allowed to identify the somatosensory gyrus posterior to the central sulcus, and on motor cortex-muscle coherence used to pinpoint the precentral motor cortex (Mäkelä *et al.,* 2001). The functional locations are displayed on 3-D reconstructions of the individual brain, with the blood vessels, derived from MR angiography, also shown on the exposed brain surface. It has turned out that the vessels are extremely important landmarks for the neurosurgeon who has to navigate in the operation area with a rather limited field of view. Intracranial recordings and direct cortical stimulations during surgery have given highly concordant results with the noninvasive preoperative MEG evaluation (Mäkelä *et al.,* 2001).

Insert Figure 20 about here.

In preoperative evaluation of epileptic patients the main questions are to find out whether the patient has local generators of epileptic discharges, where these areas are located with respect to eloquent brain areas, and in the case of multiple epileptic foci to determine the temporal relationship between the foci. For example, it is possible to identify a primary and a secondary epileptic focus on the basis of their fixed time delay, typically 20–30 ms (Barth 1993; Hari *et al.,* 1993a).

VI. Conclusions and Future Directions

With the advent of whole-head neuromagnetometers it has become evident that MEG is a valuable tool for studying both healthy and diseased human brain. The method is totally noninvasive and the measurements can be repeated as desired without risk. In contrast to PET and fMRI, MEG and EEG reflect the neural activation directly instead of indirect measures of blood flow or metabolism. Thus MEG is not hampered, for example, by haemodynamic delays, and it can track brain events at submillisecond time scale. In contrast to the EEG, the tissues outside the brain do not significantly modify the distribution of the MEG signals outside the head. Therefore, it is often easier to interpret MEG than EEG data. At best, a source having small spatial extent can be located with an accuracy of a few millimeters. In addition to source locations and orientations, MEG also provides quantitative information about activation strengths.

The main contribution to MEG signals derives from tangential and relatively superficial currents in the fissural cortex; these areas are difficult to study with other means, including even intracranial recordings. EEG is the natural companion of MEG because it provides information about radial currents as well. However, the problems in this combination arising from, *e.g.,* larger systematic errors in EEG than MEG forward modelling are still unsolved.

The signals from deep structures are attenuated both due the larger distance from the sensors to the sources and due to the effects of symmetry in the almost spherical head. Furthermore, signals from deeper structures are often masked by simultaneous activity of the cortex. Identification of deep sources reported in some MEG studies relies on accurate forward calculations and on the use of the information obtained with whole-head sensor arrays (Tesche and Karhu 1999).

In constrast to the EEG electrodes, the MEG sensor array is not fixed to the subject's head. Therefore, a head position measurement is necessary to determine the relative location and orientation of the sensor array and the subject. Even if continuous position measurements of head position were available, it may be extremely difficult to study awake young children and recordings cannot be performed during major epileptic seizures.

Present MEG instruments are designed for adult head size. However, it is conceivable that many epilepsy centers would be willing to invest to a pediatric MEG system once such devices become available.

It is important to note that MEG signals are typically evident without resorting to complicated statistical analysis apart from signal averaging. Thus it is possible to evaluate the signal quality during the data acquisition. Also, conclusions can be made on the the basis of single subject data, which allows studies of individual processing strategies. Thus grand averages, which may often be misleading, are not necessary except as a means to visualize congruent results across subjects. Furthermore, subtractions between conditions are not needed, although possible – again an important difference compared with PET and fMRI studies.

The ambiguity of the inverse problem has been often cited as a major drawback of both EEG and MEG. Both methods thus have to rely on a restrictive source model and the analysis is rather difficult for a beginner. It is also perhaps confusing to find that several competing source models are available and sometimes the authors introducing them are not clear enough in stating the underlying assumptions and their consequences for data interpretation. Constraints for the inverse problem can be obtained from other imaging modalities, for example fMRI. However, the combination fMRI–MEG is non-trivial because the two methods do not necessarily reflect directly the same brain events.

We expect major future progress in the development of efficient and automated MEG analysis methods, novel experimental paradigms to fully utilize the benefits of MEG, and reliable routines to combine MEG with other imaging modalities. We anticipate such approaches to significantly increase our understanding of human brain functions, especially their temporal dynamics.

VII. Figure Legends

Figure 1. MEG measurement setup. Left: The magnetic fields produced by neuronal currents are picked up with an array of superconducting sensors. Right: The most probable current configuration in the brain (small arrows) is calculated on the basis of the measured field pattern, in this case a current dipole model (large arrow) was used.

Figure 2. A schematic representation of currents associated with an action potential and a postsynaptic potential. Further details in text.

Figure 3. Schematic presentation of the effects of deep, radial, and tangential currents on MEG signals detected outside a spherically symmertic conductor. In all situations the external magnetic field is identical because radial currents anywhere in the sphere do not produce any external magnetic field, sources exactly in the middle of the sphere are always radial, and because concentric inhomogeneities do not affect the magnetic field. EEG would see all these currents (tangential, radial, and deep ones) but would be affected by the electric inhomogeneities.

Figure 4. The effect of the size and extension of an active cortical area in the wall of a fissure on the location of the equivalent current dipole (arrow) used to model the layer. For explanation, see text. Adapted from (Hari 1991).

Figure 5. The boundaries between the various compartments of the head employed in a boundary-element model (BEM) to calculate the potential on the surface of the head and the magnetic field outside. The surfaces have been extracted from MR images of one subject and tessellated automatically with triangles. Courtesy of Mika Seppä.

Figure 6. Strengths of various ambient and biological noise signals and of brain's biomagnetic signals, given as spectral densities as a function of frequency. Courtesy of Jukka Knuutila.

Figure 7. Different flux transformer configurations: (a) a magnetometer, (b) an axial first-order gradiometer, and (c) a first-order planar gradiometer. The plus and minus signs refer to magnetic fluxes of opposite polarities, and the arrows illustrate current directions in the wires.

Figure 8. Schematic illustration of the signal strength produced by a current dipole (at angle 0), measured outside a sphere along one line with a magnetometer (solid line) and a planar gradiometer (dashed line). Note that with a magnetometer one detects two field extrema of opposite polarities whereas the planar gradiometer picks up the maximum signal just above the dipole.

Figure 9. A subject is being prepared for a measurement with the 306-channel Vectorview™ neuromagnetometer. During the actual measurement the subject's head is covered by the helmet-shaped sensor array.

Figure 10. Examples of biological artefacts that may contaminate MEG recordings. The ballistogram time-locked to the cardiac cycle, as is inidcatged by the ECG trace below, was elicited by purpose by putting a piece of magnetic metal on the subject's abdomen

Figure 11. A comparison of minimum-norm estimates and a single current dipole used to represent a distributed source (top left) and a current dipole (top right). Note that the resulting field patterns are identical, as are the minimum norm and current dipole solutions.

Figure 12. Modelling of MEG data with the time-varying dipole model. The measured field patterns at a given time instant are explained with a linear combination of three field patterns ($\mathbf{g}_1 \ldots \mathbf{g}_3$) and additive Gaussian noise (not shown). The weights of the component field patterns are determined by the time dependencies of the dipole amplitudes ($\mathbf{q}_1 \ldots \mathbf{q}_3$) shown by curves in the lower right part of the Figure.

Figure 13. Snapshots of statistical parameter maps calculated from MEG during a verbal size judgement task in a single subject at selected latencies. The maps are based on test statistics calculated from the anatomically constrained minimum-norm estimates by normalizing them with the expected noise in the current source estimate. Activation spreads rapidly from the visual cortex, around 80 ms, to occipitotemporal, anterior temporal, and prefrontal areas. Activations are displayed on an "inflated" view of the left hemisphere with sulcal and gyral cortices shown in dark and light gray, respectively. The significance threshold for the statistical parametric maps was $p < 0.001$. Adapted from Dale et al. (2000).

Figure 14. Minimum-current estimates of brain activations in normal-hearing subjects while they viewed sign language (which they did not understand). The activation spots refer to the inferior frontal lobe (IFL; Broca's area), superior temporal sulcus (STS), and to the motion-sensititive visual area V5. Adapted from Levänen et al. (2001).

Figure 15. (a) Averaged evoked responses to electric stimulation of the right median nerve. The responses were recorded with the 204 planar gradiometers of the VectorView neuromagnetometer. The upper and lower traces of each response pair refer to latitudinal and longitudinal gradients, respectively. The dashed circles point out the areas of largest signals. (b) The corresponding field patterns at the peak latencies of the responses superimposed on the sensor array. The solid isocontours refer to magnetic flux out of the head and the dashed isocontours flux into the head. These patterns agree with activations in the left primary somatosensory cortex SI and in the second somatosensory cortices of both hemispheres. Stimulus artifacts at time 0 are seen on several left-sided channels.

Figure 16. (a) The current dipole sources identified for the signals of Figure 15, superimposed on the MRI slices of the same subject. The dots refer to the source locations (which agree with activations of the left SI and of the bilateral SII cortices) and the bars show the directions of the source currents; note that the intracellular current flow is restricted to the cortex. (b) Source strengths as a function of time, derived from a 4-dipole model, with two sources in the left SI and one source in the SII cortex of each hemisphere. The lowest trace indicates the goodness of fit of the model in explaining all the 204-channel responses as a function of time.

Figure 17. Cortex-muscle coherence. (a) Surface electromyogram from isometrically contracted foot muscle and the simultaneously measured MEG signal over the motor foot area. (b) Coherence spectra between MEG and rectified EMG from isometrically contracted right and left hand muscles (upper and lower spectra, respectively). The horizontal dashed line indicates the 99% significance level. The schematic heads on the right show the spatial locations of MEG signals corresponding to the strongest peaks in the coherence spectra. Adapted from Salenius *et al.* (1997b).

Figure 18. Top: The main source locations for one subject while he was executing, imitating (online), and observing reaching hand movements. Each movement ended with pinching the top of a manipulandum which gave an triggering pulse to signal averaging. In the control condition, the hand approached the manipulandum without pinching. The sources are superimposed on the subject's own three-dimenzsional MRI brain surface, viewed from left and right sides. Bottom, left: Strengths of the main four dipoles in the inferior frontal (IFA) and the occipital (Occ) area of the left hemisphere, and in the motor cortices (M1) of both hemispheres as a function of time; a 4-dipole time-varying model was used to explain the data during all conditions. Bottom, right: Mean (± SEM) peak latencies of source waveforms in all source areas. Adapted from Nishitani and Hari (2000a).

Figure 19. Schematic presentation of auditory pathways. The red and blue lines illustrate the left- and right-ear inputs to the auditory cortices; the amplitudes of the corresponding sounds were modulated at 26.1 and 20.1 Hz (AM depth 80%), respectively. The sources of the measured MEG signals are shown as current dipoles in the auditory cortices of both hemispheres. Middle: Frequency spectra (resolution 0.074 Hz) from signals measured over each auditory cortex of one subject. Left-ear sounds elicited spectral peaks at 26.1 Hz and the right-ear at 20.1 Hz in both hemispheres; both signals were suppressed during binaural listening. Adapted from Fujiki et al. (2001).

Figure 20. Identification of the central sulcus in a patient who has brain tumor in the right parietal lobe. The postcentral somatosensory cortex was identified on the basis of source locations for somatosensory responses to electric stimulation of hand and foot nerves, and the precentral motor cortex was identified on the basis of sources of the cortex–muscle coherence for upper and lower limb muscles. The surface rendering on the right also shows cortical veins which serve as landmarks for the neurosurgeon during operation.

VIII. References

Ahonen, A.I., Hämäläinen, M.S., Ilmoniemi, R.J., Kajola, M.J., Knuutila, J.E., Simola, J.T., and Vilkman, V.A. (1993). Sampling theory for neuromagnetic detector arrays. *IEEE Trans. Biomed. Eng.*, **40,** 859-869.

Aine, C., Huang, M., Stephen, J., and Christner, R. (2000). Multistart algorithms for MEG empirical data analysis reliably characterize locations and time courses of multiple sources. *Neuroimage*, **12,** 159-72.

Allison, T., McCarthy, G., Wood, C., Williamson, P., and Spencer, D. (1989). Human cortical potentials evoked by stimulation of the median nerve. II. Cytoarchitectonic areas generating long-latency activity. *J. Neurophysiol.*, **62,** 711-722.

Amidzic, O., Riehle, H.J., Fehr, T., Wienbruch, C., and Elbert, T. (2001). Pattern of focal gamma-bursts in chess players. *Nature*, **412,** 603.

Antervo, A., Hari, R., Katila, T., Ryhänen, T., and Seppänen, M. (1985). Magnetic fields produced by eye blinking. *Electroenceph. Clin. Neurophysiol.*, **61,** 247-254.

Barnard, A.C., Duck, I.M., and Lynn, M.S. (1967). The application of electromagnetic theory to electrocardiology. I. Derivation of the integral equations. *Biophys. J.*, **7,** 443-462.

Barth, D.S. (1993). The neurophysiological basis of epileptiform magnetic fields and localization of neocortical sources. *J. Clin. Neurophysiol.*, **10,** 99-107.

Berg, P., and Scherg, M. (1996). Sequential brain source imaging: evaluation of localization accuracy. *In* "Recent Advances in Event-Related Brain Potential Research" (C. Ogura, Y. Coga, M. Shimokochi, eds.). pp. Elsevier, Amsterdam.

Bernander, O., Douglas, R., Martin, K., and Koch, C. (1991). Synaptic background activity determined spatial-temporal integration in pyramidal cells. *Proc. Natl. Acad. Sci. USA*, **88,** 11569-11573.

Bowyer, S.M., Tepley, N., Papuashvili, N., Kato, S., Barkley, G.L., Welch, K.M., and Okada, Y.C. (1999). Analysis of MEG signals of spreading cortical depression with propagation constrained to a rectangular cortical strip. II. Gyrencephalic swine model. *Brain Res.*, **843,** 79-86.

Brebbia, C., Telles, J., and Wrobel, L. (1984). "Boundary Element Techniques – Theory and Applications in Engineering". Springer-Verlag, Berlin.

Brown, P., Salenius, S., Rothwell, J.C., and Hari, R. (1998). The cortical correlate of the Piper rhythm in man. *J. Neurophysiol.*, **80,** 2911-2917.

Brown, R.J., Candy, T.R., and Norcia, A.M. (1999). Development of rivalry and dichoptic masking in human infants. *Invest. Ophthalmol. Vis. Sci.*, **40,** 3324-3333.

Buchner, H., Knoll, G., Fuchs, M., Rienacker, A., Beckmann, R., Wagner, M., Silny, J., and Pesch, J. (1997). Inverse localization of electric dipole current sources in finite element models of the human head. *Electroencephalogr. Clin. Neurophysiol.*, **102,** 267-278.

Carelli, P., and Leoni, R. (1986). Localization of biological sources with arrays of superconducting gradiometers. *J. Appl. Phys.*, **59,** 645-650.

Clarke, J., Goubau, W.M., and Ketchen, M.B. (1976). Tunnel junction dc SQUID fabrication, operation, and performance. *J. Low Temp. Phys.*, **25,** 99-144.

Cohen, D. (1968). Magnetoencephalography: evidence of magnetic field produced by alpha-rhythm currents. *Science*, **161,** 784-786.

Cohen, D. (1970). Low-field room built at high-field magnet lab. *Physics Today*, **23,** 56-57.

Cohen, D. (1972). Magnetoencephalography: detection of the brain's electrical activity with a superconducting magnetometer. *Science*, **175,** 664-666.

Cohen, D. (1979). Magnetic measurement and display of current generators in the brain. Part I: The 2-D detector. *In* "12th Intl. Conf. on Medical and Biological Eng." eds.). pp. 15. Petah Tikva, Beilinson Medical Center, Jerusalem.

Conway, B., Halliday, D., Farmer, S., Shahani, U., Maas, P., Weir, A., and Rosenberg, J. (1995). Synchronization between motor cortex and spinal motoneuronal pool during the performance of a maintained motor task in man. *J. Physiol.*, **489,** 917-924.

Curio, G., Mackert, B., Burghoff, M., Koetiz, R., Abraham-Fuchs, K., and Harer, W. (1994). Localization of evoked neuromagnetic 600 Hz activity in the cerebral somatosensory system. *Electroenceph. Clin. Neurophysiol.*, **91,** 483-487.

Dale, A.M., Fischl, B., and Sereno, M.I. (1999). Cortical surface-based analysis. I. Segmentation and surface reconstruction. *Neuroimage*, **9,** 179-194.

Dale, A.M., Liu, A.K., Fischl, B.R., Buckner, R.L., Belliveau, J.W., Lewine, J.D., and Halgren, E. (2000). Dynamic statistical parametric mapping: combining fMRI and MEG for high-resolution imaging of cortical activity. *Neuron*, **26,** 55-67.

Dale, A.M., and Sereno, M.I. (1993). Improved localization of cortical activity by combining EEG and MEG with MRI cortical surface reconstruction: A linear approach. *J. Cogn. Neurosci.*, **5,** 162-176.

Erné, S., Curio, G., Trahms, L., Trontelj, Z., and Aust, P. (1988). Magnetic activity of a single peripheral nerve in man. *In* "Biomagnetism '87" (K. Atsumi, M. Kotani, S. Ueno, T. Katila, S. Williamson, eds.). pp. 166-169. Tokyo Denki University Press, Tokyo.

Erné, S.N., Hahlbohm, H.D., Scheer, H., and Trontelj, Z. (1981). The Berlin magnetically shielded room (BMSR): Section B - performances. *In* "Biomagnetism" (S.N. Erné, H.-D. Hahlbohm, H. Lubbig, eds.). pp. 79-87. Walter de Gruyter, Berlin.

Erné, S.N., Narici, L., Pizzella, V., and Romani, G.L. (1987). The positioning problem in biomagnetic measurements: A solution for arrays of superconducting sensors. *IEEE Trans. Magn.*, **MAG-23,** 1319-1322.

Fadiga, L., Fogassi, L., Pavesi, G., and Rizzolatti, G. (1995). Motor facilitation during action observation: A magnetic stimulation study. *J. Neurophysiol.*, **73,** 2608-2611.

Fischl, B., Sereno, M.I., and Dale, A.M. (1999). Cortical surface-based analysis. II: Inflation, flattening, and a surface-based coordinate system. *Neuroimage*, **9,** 195-207.

Forss, N., Salmelin, R., and Hari, R. (1994). Comparison of somatosensory evoked fields to airpuff and electric stimuli. *Electroenceph. Clin. Neurophysiol.*, **92,** 510-517.

Forss, N., Silén, T., and Karjalainen, T. (2001). Lack of activation of human secondary somatosensory cortex in Unverricht-Lundborg type of progressive myoclonus epilepsy. *Ann. Neurol.*, **49,** 90-97.

Fuchs, M., Wagner, M., Köhler, T., and Wischmann, H.-A. (1999). Linear and nonlinear current density reconstructions. *J. Clin. Neurophysiol.*, **16,** 267-295.

Fujiki, N., Jousmäki, V., and Hari , R. (2001). Tagging auditory inputs during binaural hearing. *J. Neurosci.*, under revision.

Geselowitz, D. (1970). On the magnetic field generated outside an inhomogeneous volume conductor by internal current sources. *IEEE Trans. Magn.*, **MAG-6,** 346-347.

Gross, J., Kujala, J., Hämäläinen, M., Timmermann, L., Schnitzler, A., and Salmelin, R. (2001). Dynamic imaging of coherent sources: Studying neural interactions in the human brain. *Proc. Natl. Acad. Sci. USA*, **98,** 694-699.

Gross, J., Tass, P.A., Salenius, S., Hari, R., Freund, H., and Schnitzler, A. (2000). Cortico-muscular synchronization during isometric muscle contraction in humans as revealed by magnetoencephalography. *J. Physiol.*, **527,** 623-631.

Halgren, E., Liu, A., Ulbert, I., Klopp, J., Heit, G., and Dale, A. (2000). Fron synapse to sensor: How much of the EEG/MEG signal is waylaid by spatiotemporal asynchronies? *Book of Abstracts, 12th International Conference on Biomagnetism*, 36a.

Hämäläinen, M., Hari, R., Ilmoniemi, R., Knuutila, J., and Lounasmaa, O.V. (1993). Magnetoencephalography – theory, instrumentation, and applications to noninvasive studies of the working human brain. *Rev. Mod. Physics*, **65,** 413-497.

Hämäläinen, M., and Ilmoniemi, R. (1984). Interpreting magnetic fields of the brain: minimum norm estimates. Report TKK-F-A559, Helsinki University of Technology, Espoo.

Hämäläinen, M., and Ilmoniemi, R. (1994). Interpreting magnetic fields of the brain: minimum norm estimates. *Medical & Biological Engineering & Computing*, **32,** 35-42.

Hämäläinen, M.S., and Sarvas, J. (1989). Realistic conductivity geometry model of the human head for interpretation of neuromagnetic data. *IEEE Trans. Biomed. Eng.*, **BME-36,** 165-171.

Hansen, P.C. (1992). Analysis of discrete ill-posed problems by means of the L-curve. *SIAM Review*, **34,** 561-580.

Hari, R. (1991). On brain's magnetic responses to sensory stimuli. *J. Clin. Neurophysiol.*, **8,** 157-169.

Hari, R. (1999). Magnetoencephalography as a tool of clinical neurophysiology. *In* "Electroencephalography. Basic Principles, Clinical Applications and Related Fields. 4th ed. Chapter 60." (E. Niedermeyer, F. Lopes da Silva, eds.). pp. 1107-1134. Williams & Wilkins,

Hari, R., et al. (1993a). Parietal epileptic mirror focus detected with a whole-head neuromagnetometer. *NeuroReport*, **5,** 45-48.

Hari, R., and Forss, N. (1999). Magnetoencephalography in the study of human somatosensory cortical processing. *Proc. Royal. Soc. Lond. B*, **354,** 1145-1154.

Hari, R., Forss, N., Avikainen, S., Kirveskari, E., Salenius, S., and Rizzolatti, G. (1998). Activation of human primary motor cortex during action observation: A neuromagnetic study. *Proc. Natl. Acad. Sci. USA*, **95,** 15061-15065.

Hari, R., Hällström, J., Tiihonen, J., and Joutsiniemi, S. (1989). Multichannel detection of magnetic compound action fields of median and ulnar nerves. *Electroenceph. Clin. Neurophysiol.*, **72,** 277-280.

Hari, R., Karhu, J., Hämäläinen, M., Knuutila, J., Salonen, O., Sams, M., and Vilkman, V. (1993b). Functional organization of the human first and second somatosensory cortices: A neuromagnetic study. *Eur. J. Neurosci.*, **5,** 724-734.

Hari, R., Levänen, S., and Raij, T. (2000). Timing of human cortical activation sequences during cognition: role of MEG. *Trends Cogn. Sci.*, **4,** 455-462.

Hari, R., and Salmelin, R. (1997). Human cortical rhythms: a neuromagnetic view through the skull. *Trends Neurosci.*, **20,** 44-49.

Hari, R., Salmelin, R., Mäkelä, J.P., Salenius, S., and Helle, M. (1997). Magnetoencephalographic cortical rhythms. *Int. J. Psychophysiol.*, **26,** 51-62.

Hashimoto, I., Mashiko, T., and Imada, T. (1996). Somatic evoked high-frequency magnetic oscillations reflect activity of inhibitory interneurons in the human somatosensory cortex. *Electroenceph. Clin. Neurophysiol.*, **100,** 189-203.

Helmholtz, H. (1953). Ueber einige Gesetze der Vertheilung elektrischer Ströme in körperlichen Leitern, mit Anwendung auf die thierisch-elektrischen Versuche. *Ann. Phys. Chem.*, **89,** 211.

Horacek, B.M. (1973). Digital model for studies in magnetocardiography. *IEEE Trans. Magn.*, **MAG-9,** 440-444.

Huang, M.X., Aine, C., Davis, L., Butman, J., Christner, R., Weisend, M., Stephen, J., Meyer, J., Silveri, J., Herman, M., and Lee, R.R. (2000). Sources on the anterior and posterior banks of the central sulcus identified from magnetic somatosensory evoked responses using multistart spatio-temporal localization. *Hum. Brain Mapp.*, **11,** 59-76.

Iacoboni, M., Woods, R.P., Brass, M., Bekkering, H., Mazziotta, J.C., and Rizzolatti, G. (1999). Cortical mechanisms of human imitation. *Science*, **286,** 2526-8.

Ioannides, A.A., Bolton, J.P.R., and Clarke, C.J.S. (1990). Continuous probabilistic solutions to the biomagnetic inverse problem. *Inverse Problems*, **6,** 523-542.

Jenkins, G., and Watts, D. (1968). "Spectral Analysis and its Applications". Holden-Day, San Francisco.

Josephson, B.D. (1962). Possible new effects in superconductive tunnelling. *Phys. Lett*, **1,** 251-253.

Jousmäki, V., and Hari, R. (1996). Cardiac artifacts in magnetoencephalogram. *J. Clin. Neurophysiol.*, **13,** 172-176.

Katila, T.E. (1983). On the current multipole presentation of the primary current distributions. *Nuovo Cimento*, **2D,** 660-664.

Kelhä, V.O., Pukki, J.M., Peltonen, R.S., Penttinen, A.J., Ilmoniemi, R.J., and Heino, J.J. (1982). Design, construction, and performance of a large volume magnetic shield. *IEEE Trans. Magn.*, **18,** 260-270.

Knuutila, J., Ahonen, A., Hämäläinen, M., Kajola, M., Laine, P., Lounasmaa, O., Parkkonen, L., Simola, J., and Tesche, C. (1993). A 122-channel whole-cortex SQUID system for measuring the brain's magnetic fields. *IEEE Trans. Magn.*, **29,** 3315-3320.

Knuutila, J., Ahonen, A.I., Hämäläinen, M.S., Ilmoniemi, R.J., and Kajola, M.J. (1985). Design considerations for multichannel SQUID magnetometers. *In* "SQUID'85: Superconducting Quantum Interference Devices and their Applications" (H.D. Hahlbohm, H. Lubbig, eds.). pp. 939-944. Walter de Gruyter, Berlin.

Levänen, S., Uutela, K., Salenius, S., and Hari, R. (2001). Cortical representation of observed signs: Comparison of deaf signers and hearing non-signers. *Cereb. Cortex*, **11,** 506-512.

Lötjönen, J., Magnin, I.E., Nenonen, J., and Katila, T. (1999a). Reconstruction of 3-D geometry using 2-D profiles and a geometric prior model. *IEEE Trans. Med. Imaging*, **18,** 992-1002.

Lötjönen, J., Reissman, P.J., Magnin, I.E., and Katila, T. (1999b). Model extraction from magnetic resonance volume data using the deformable pyramid. *Med. Image. Anal.*, **3,** 387-406.

Lounasmaa, O.V. (1974). "Experimental Principles and Methods below 1K". Academic Press, London.

Lounasmaa, O.V., Hämäläinen, M., Hari, R., and Salmelin, R. (1996). Information processing in the human brain – magnetoencephalographic approach. *Proc. Natl. Acad. Sci. USA*, **93,** 8809-8815.

Mäkelä, J., et al. (2001). Three-dimensional integration of brain anatomy and function to facilitate intraoperative navigation around the sensorimotor strip. *Hum. Brain Mapp.*, **12,** 180-192.

Marquardt, D.W. (1963). An algorithm for least-squares estimation of nonlinear parameters. *J. Soc. Indust. Appl. Math*, **11,** 431-441.

Matsuura, K., and Okabe, Y. (1997). A robust reconstruction of sparse biomagnetic sources. *IEEE Trans. Biomed. Eng.*, **44,** 720-726.

Mosher, J., Lewis, P., and Leahy, R. (1992). Multiple dipole modeling and localization from spatio-temporal MEG data. *IEEE Trans. Biomed. Eng.*, **39,** 541-557.

Mosher, J.C., and Leahy, R.M. (1998). Recursive MUSIC: a framework for EEG and MEG source localization. *IEEE Trans. Biomed. Eng.*, **45,** 1342-1354.

Mosher, J.C., and Leahy, R.M. (1999). Source localization using recursively applied and projected (RAP) MUSIC. *IEEE Trans. Signal Proc.*, **47,** 332-340.

Mosher, J.C., Leahy, R.M., Shattuck, D.W., and Baillet, S. (1999). MEG source imaging using multipolar expansions. *In* "IPMI99" (A. Kua, eds.). pp. 98-111. Springer-Verlag, Hungary.

Murayama, N., Lin, Y.-Y., Salenius, S., and Hari, R. (2001). Oscillatory interaction between human motor cortex and trunk muscles during isometric contraction. *Neuroimage*, in press.

Näätänen, R., Ilmoniemi, R., and Alho, K. (1994). Magnetoencephalography in studies of human cognitive brain function. *Trends Neurosci.*, **17,** 389-395.

Nishitani, N., and Hari, R. (2000a). Temporal dynamics of cortical representation for action. *Proc. Natl. Acad. Sci. USA*, **97,** 913-918.

Nishitani, N., and Hari, R. (2000b). Temporal dynamics of human cortical activities related to recognition of lip forms. *Book of Abstracts, 12th International Conference on Biomagnetism*, 108a.

Nolte, G., and Curio, G. (2000). Current multipole expansion to estimate lateral extent of neuronal activity: a theoretical analysis. *IEEE Trans. Biomed. Eng.*, **47,** 1347-1355.

Okada, Y., Wu, J., and Kyuhou, S. (1997). Genesis of MEG signals in a mammalian CNS structure. *Electroenceph. Clin. Neurophysiol.*, **103,** 474-485.

Okada, Y.C., Lähteenmäki, A., and Xu, C. (1999). Experimental analysis of distortion of magnetoencephalography signals by the skull. *Clin. Neurophysiol.*, **110,** 230-238.

Oppenheim, A., and Schafer, R. (1975). "Digital Signal Processing". Prentice Hall, Englewood Cliffs.

Pascual-Marqui, R.D., Michel, C.M., and D, L. (1995). Low resolution electromagnetic tomography: a new method for localizing electrical activity in the brain. *Int. J. Psychophysiol.*, **18,** 49-65.

Patel, A.D., and Balaban, E. (2000). Temporal patterns of human cortical activity reflect tone sequence structure. *Nature*, **404,** 80-84.

Pfurtscheller, G. (1992). Event-related synchronization (ERS): an electrophysiological correlate of cortical areas at rest. *Electroenceph. Clin. Neurophysiol.*, **83,** 62-69.

Pfurtscheller, G., and Aranibar, A. (1977). Event-related desynchronization detected by power measurements of scalp EEG. *Electroenceph. Clin. Neurophysiol.*, **42,** 138-146.

Plonsey, R. (1969). "Bioelectric phenomena". McGraw-Hill, New York.

Quiroga, R.Q., and Schürmann, M. (1999). Functions and sources of event-related EEG alpha oscillations studied with the wavelet transform. *Clin. Neurophysiol.*, **110,** 643-654.

Rizzolatti, G., Fadiga, L., Gallese, V., and Fogassi, L. (1996a). Premotor cortex and recognition of motor actions. *Cogn. Brain Res.*, **3,** 131-141.

Rizzolatti, G., Fadiga, L., Matelli, M., Bettinardi, V., Paulesu, E., Perani, D., and Fazio, F. (1996b). Localization of grasp representations in humans by PET. Observation versus execution. *Exp. Brain. Res.*, **111,** 246-252.

Ryhänen, T., Seppä, H., Ilmoniemi, R., and Knuutila, J. (1989). SQUID magnetometers for low-frequency applications. *J. Low Temp. Phys*, **76,** 287-386.

Salenius, S., Forss, N., and Hari, R. (1997a). Rhythmicity of descending motor commands covaries with the amount of motor cortex 20–30 Hz rhythms. *Soc. Neurosci. Abstr.*, **23,** 1948.

Salenius, S., Portin, K., Kajola, M., Salmelin, R., and Hari, R. (1997b). Cortical control of human motoneuron firing during isometric contraction. *J. Neurophysiol.*, **77,** 3401-3405.

Salmelin, R., Hämäläinen, M., Kajola, M., and Hari, R. (1995). Functional segregation of movement-related rhythmic activity in the human brain. *Neuroimage*, **2,** 237-243.

Salmelin, R., and Hari, R. (1994). Spatiotemporal characteristics of rhythmic neuromagnetic activity related to thumb movement. *Neurosci.*, **60,** 537-550.

Sarvas, J. (1987). Basic mathematical and electromagnetic concepts of the biomagnetic inverse problem. *Phys. Med. Biol.*, **32,** 11-22.

Scherg, M. (1990). Fundamentals of dipole source potential analysis. *In* "Auditory Evoked Magnetic Fields and Potentials" (F. Grandori, M. Hoke, G.L. Romani, eds.). pp. 40-69. Karger, Basel.

Scherg, M., and von Cramon, D. (1985). Two bilateral sources of the late AEP as identified by a spatio-temporal dipole model. *Electroenceph. Clin. Neurophysiol.*, **62,** 232-244.

Schiff, S.J., Aldroubi, A., Unser, M., and Sato, S. (1994). Fast wavelet transformation of EEG. *Electroenceph. Clin. Neurophysiol.*, **91,** 442-55.

Schmidt, D.M., George, J.S., and Wood, C.C. (1999). Bayesian inference applied to the electromagnetic inverse problem. *Hum. Brain. Mapp.*, **7,** 195-212.

Schmidt, R. (1986). Multiple emitter location and signal parameter estimation. *IEEE Trans. Ant. Propag.*, **AP-34,** 276-280.

Schmolesky, M.T., Wang, Y., Hanes, D.P., Thompson, K.G., Leutgeb, S., Schall, J.D., and Leventhal, A.G. (1998). Signal timing across the macaque visual system. *J. Neurophysiol.*, **79,** 3272-3278.

Schnitzler, A., Salenius, S., Salmelin, R., Jousmäki, V., and Hari, R. (1995). Involvement of primary somatomotor cortex in motor imagery: a neuromagnetic study. *Soc. Neurosci. Abstr.*, **21,** 518.

Singh, K.D., Holliday, I.E., Furlong, P.L., and Harding, G.F.A. (1997). Evaluation of MRI-MEG/EEG co-registration strategies using Monte Carlo simulation. *Electroenceph. Clin. Neurophysiol.*, **102,** 81-85.

Strafella, A.P., and Paus, T. (2000). Modulation of cortical excitability during action observation: a transcranial magnetic stimulation study. *Neuroreport*, **11,** 2289-92.

Tarantola, A. (1987). "Inverse Problem Theory". Elseview, New York.

Tesche, C., et al. (1985). Practical dc SQUIDs with extremely low 1/f noise. *IEEE Trans. Magn.*, **MAG-21,** 1032-1035.

Tesche, C.D., and Karhu, J. (1999). Interactive processing of sensory input and motor output in the human hippocampus. *J. Cogn. Neurosci.*, **11,** 424-436.

Tuomisto, T., Hari, R., Katila, T., Poutanen, T., and Varpula, T. (1983). Studies of auditory evoked magnetic and electric responses: modality specificity and modelling. *Nuovo Cimento*, **2D,** 471-494.

Uusitalo, M., and Ilmoniemi, R. (1997). Signal-space projection method for separating MEG and EEG into components. *Med. Biol. Eng. Comp.*, **35,** 135-140.

Uutela, K., Hämäläinen, M., and Salmelin, R. (1998). Global optimization in the localization of neuromagnetic sources. *IEEE Trans. Biomed. Eng.*, **45,** 716-723.

Uutela, K., Hämäläinen, M., and Somersalo, E. (1999). Visualization of magnetoencephalographic data using minimum current estimates. *Neuroimage*, **10,** 173-180.

Uutela, K., Taulu, S., and Hämäläinen, M. (2001). Detecting and correcting for head movements in neuromagnetic measurements. *Neuroimage*, **14,** in press.

Vieth, J.B., Kober, H., and Grummich, P. (1996). Sources of spontaneous slow waves associated with brain lesions, localized by using the MEG. *Brain Topogr.*, **8,** 215-221.

Wikswo, J.P., Barach, J.P., and Freeman, J.A. (1980). Magnetic field of a nerve impulse: first measurements. *Science*, **208,** 53-55.

Wikswo, J.P., Jr., and van Egeraat, J.M. (1991). Cellular magnetic fields: Fundamental and applied measurements on nerve axons, peripheral nerve bundles, and skeletal muscle. *J. Clin. Neurophysiol.*, **8,** 170-188.

Wu, J., and Okada, Y.C. (2000). Roles of calcium- and voltage-sensitive potassium currents in the generation of neuromagnetic signals and field potentials in a CA3 longitudinal slice of the guinea-pig. *Clin. Neurophysiol.*, **111,** 150-60.

Zhang, Z. (1995). A fast method to compute surface potentials generated by dipoles within multilayer anisotropic spheres. *Phys. Med. Biol.*, **40,** 335-349.

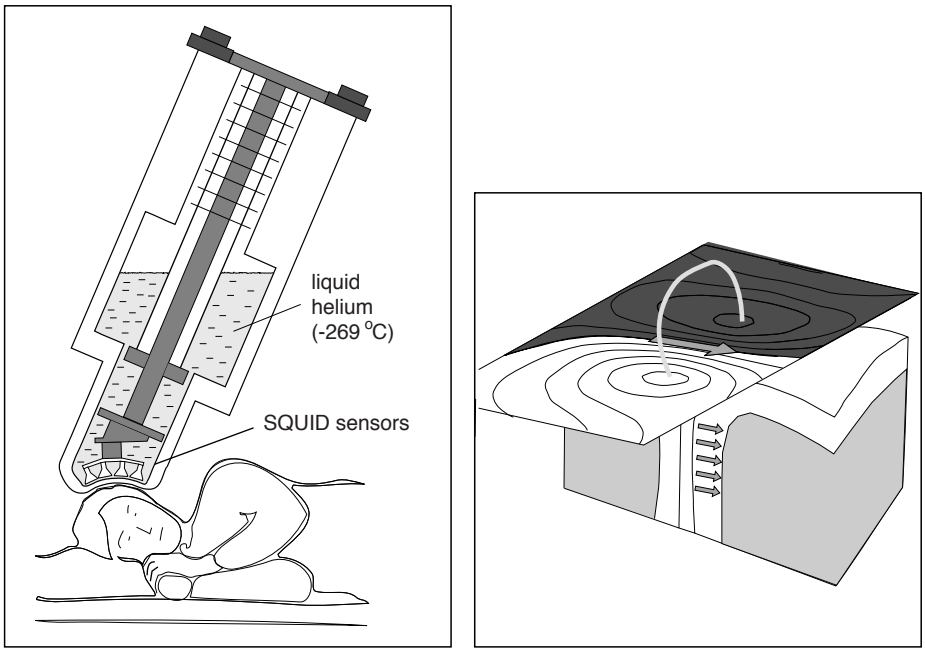

Hämäläinen and Hari, Fig 1.

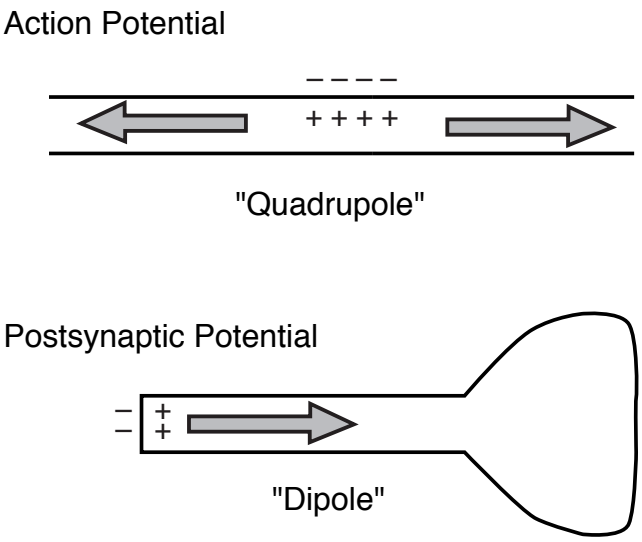

Hämäläinen and Hari, Fig 2
(one column)

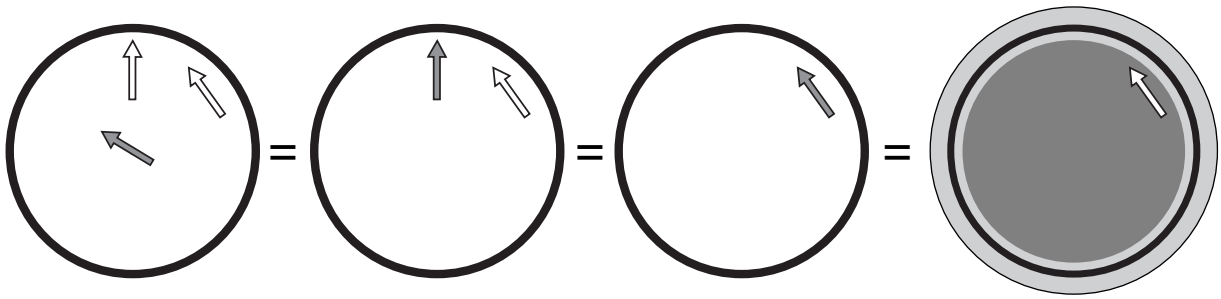

Hämäläinen and Hari, Fig 3
(two columns)

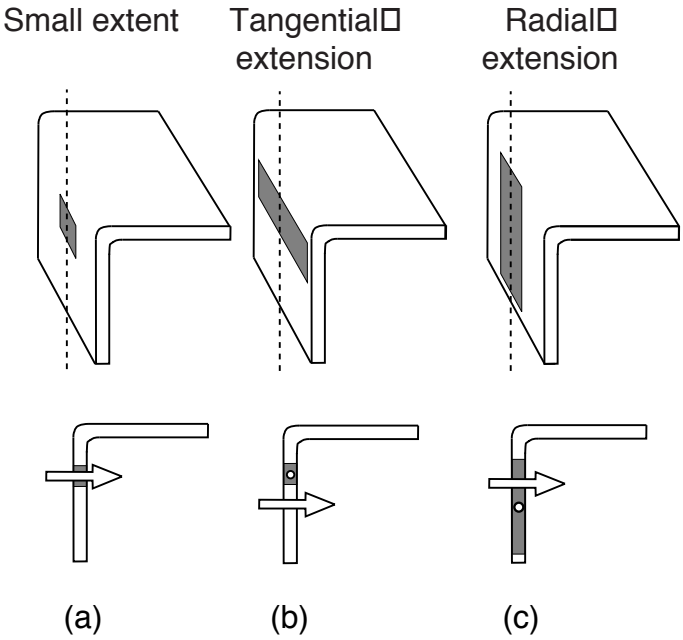

Hämäläinen and Hari, Fig 4
(one column)

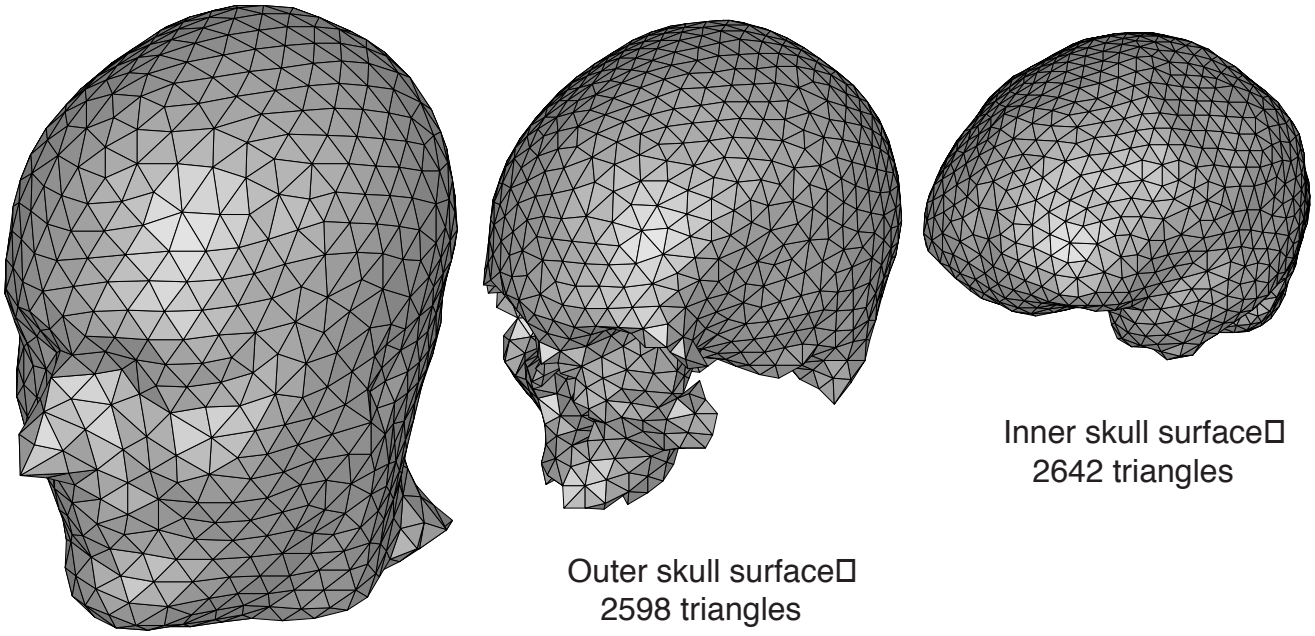

Skin surface
1926 triangles

Outer skull surface
2598 triangles

Inner skull surface
2642 triangles

Hämäläinen and Hari, Fig 5.
(two columns)

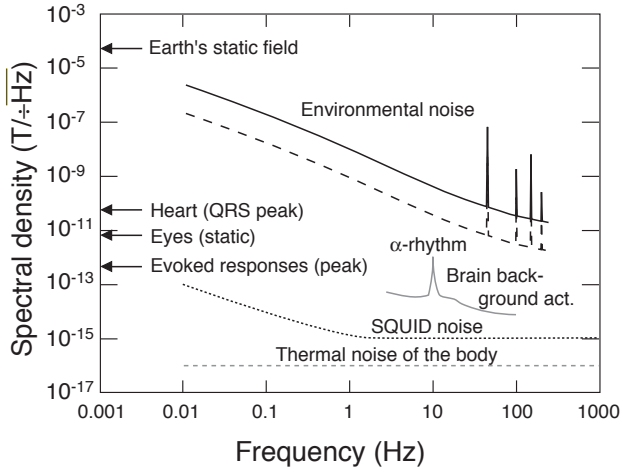

Hämäläinen and Hari, Fig 6
(one column)

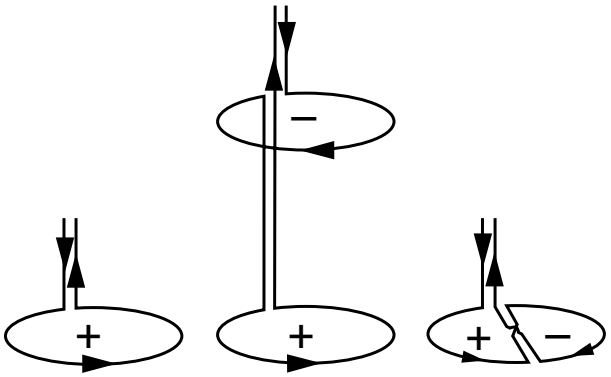

Hämäläinen and Hari, Fig 7
(one column)

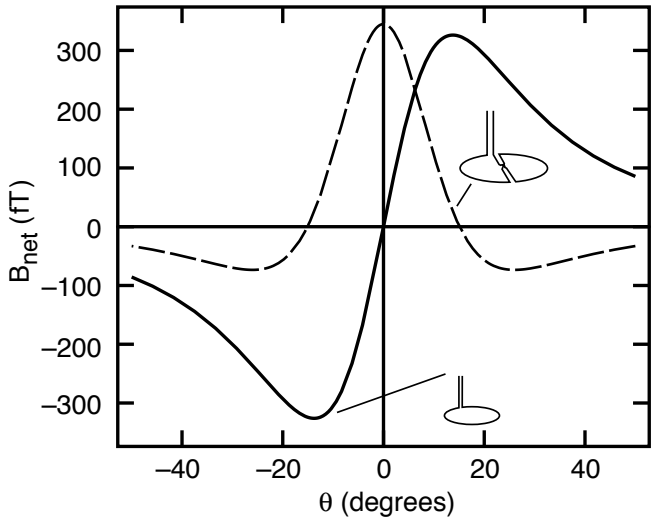

Hämäläinen and Hari, Fig 8□
(one column)


VECTORVIEW

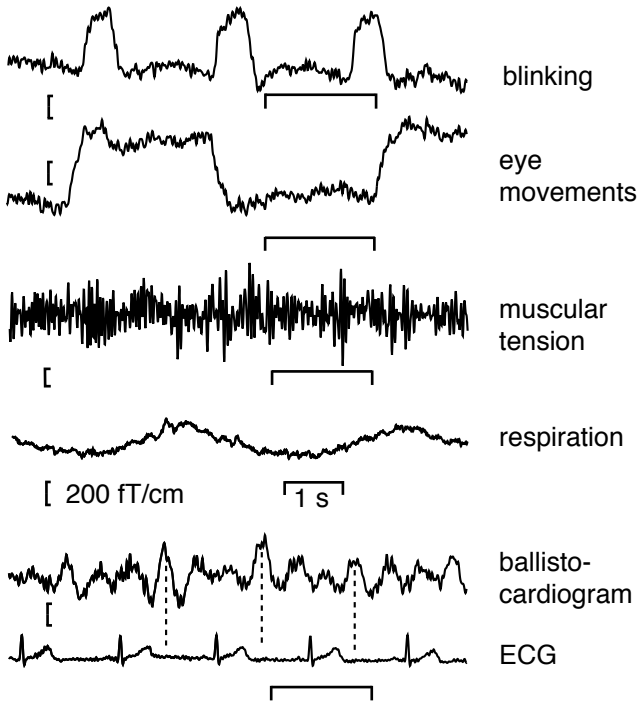

Hämäläinen and Hari, Fig 10
(one column)

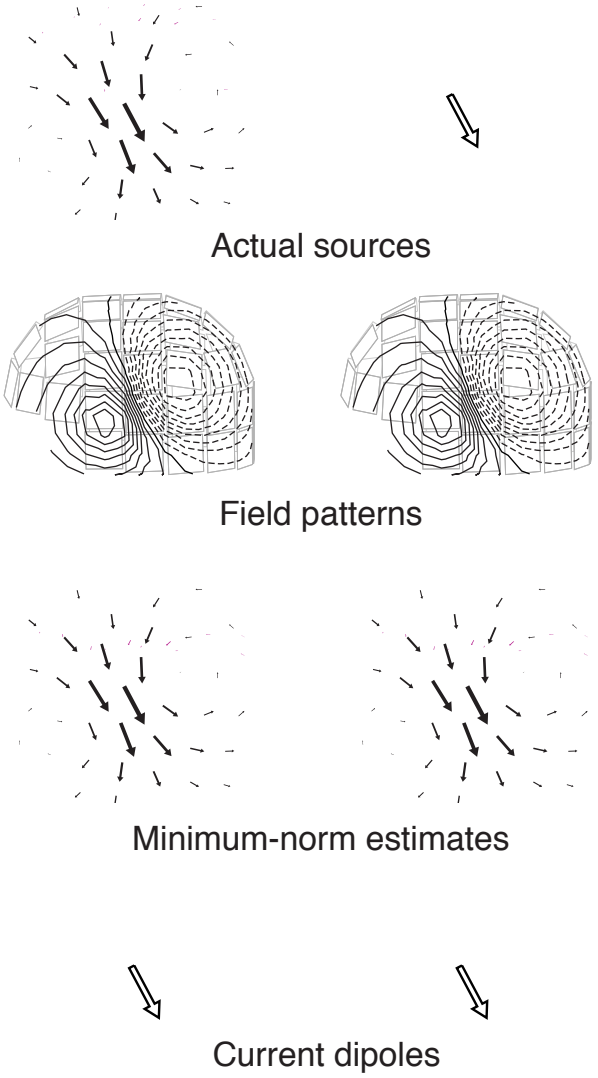

Hämäläinen and Hari, Fig 11
(one column)

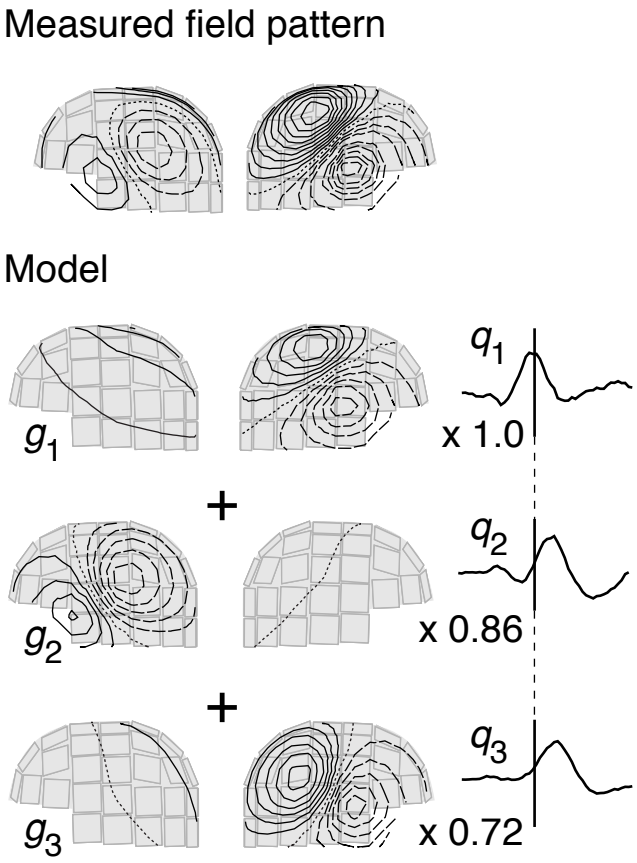

Hämäläinen and Hari, Fig 12
(one column)

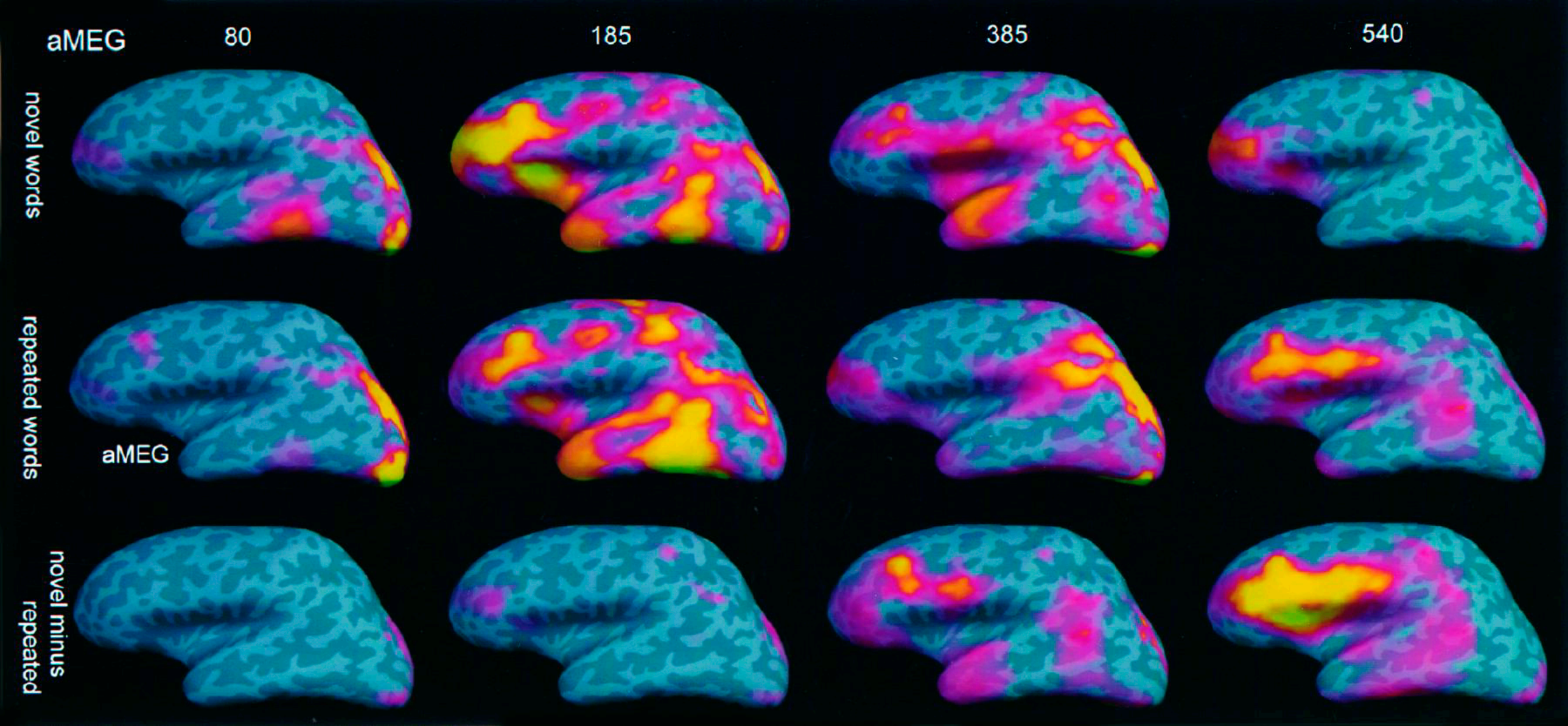
aMEG
80
185
385
540
novel words
repeated words
aMEG
novel minus repeated

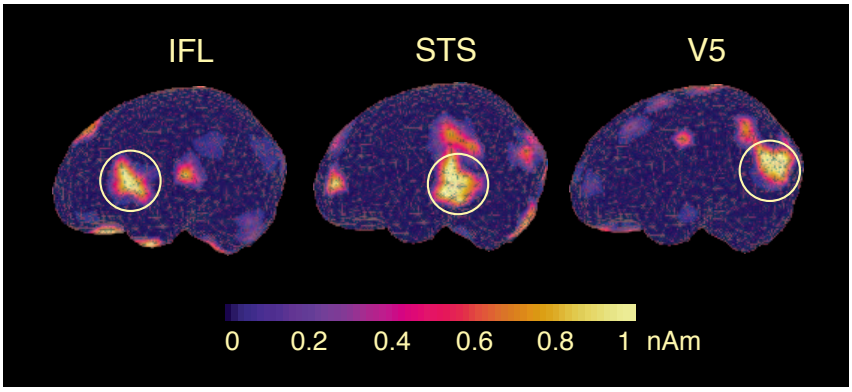

Hämäläinen and Hari, Fig 14

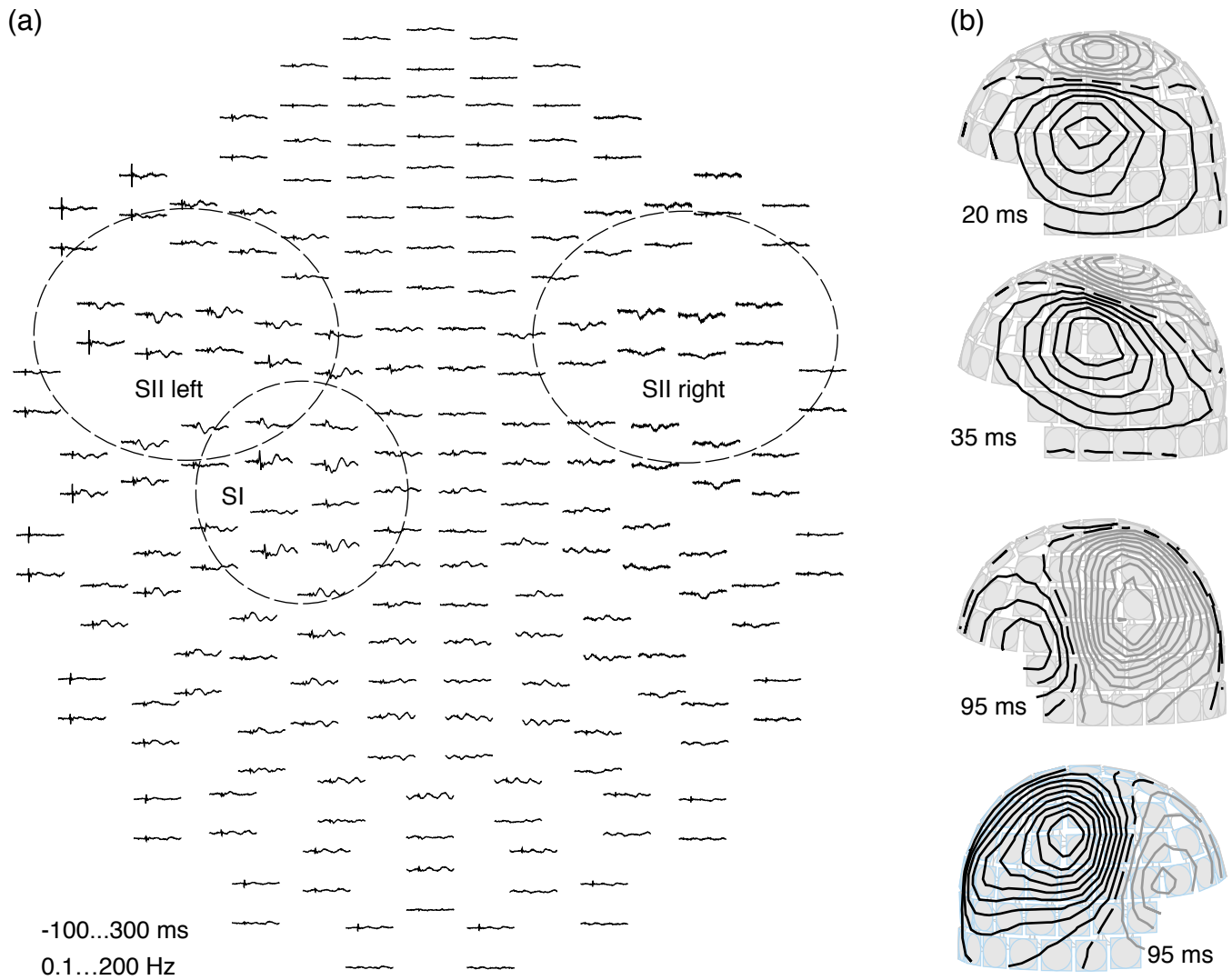

Hämäläinen and Hari, Fig 15

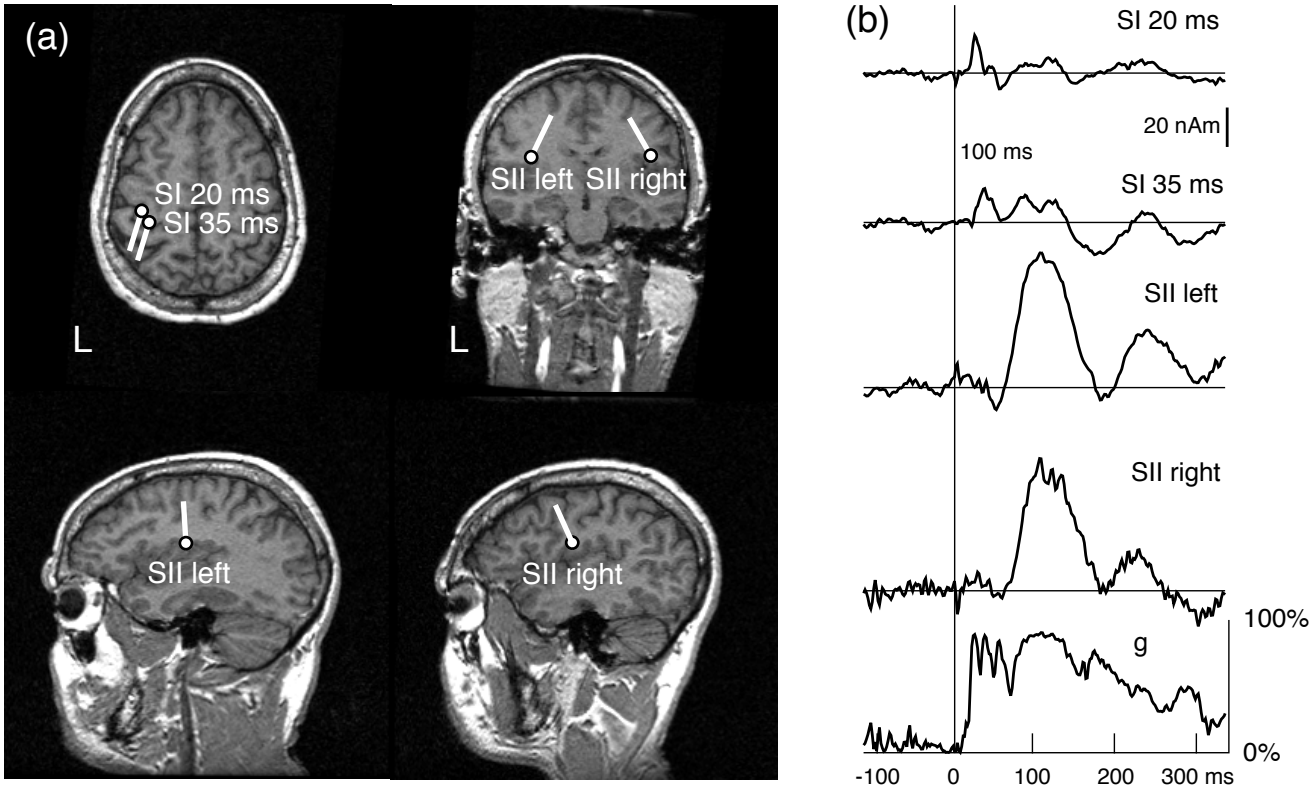

Hämäläinen and Hari, Fig 16

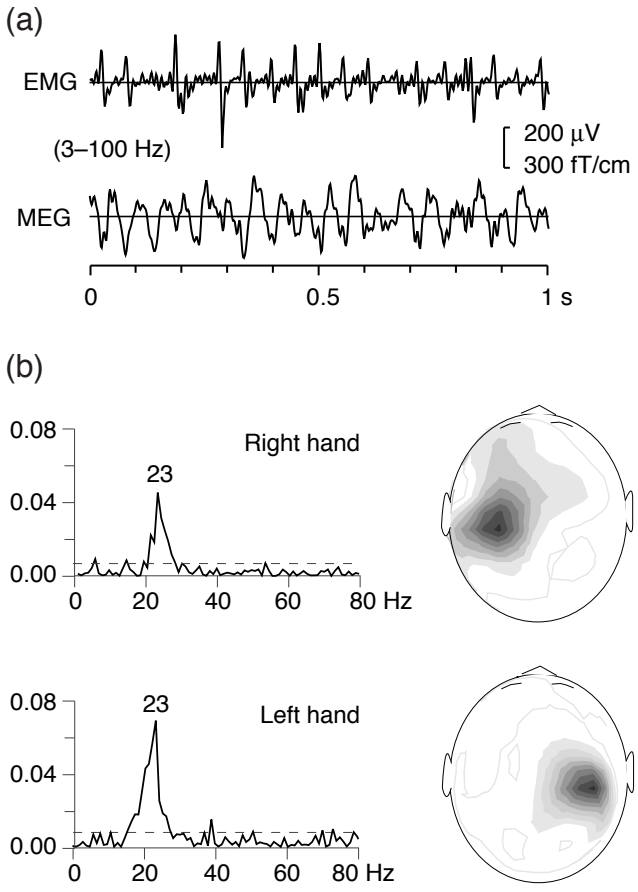

Hämäläinen and Hari, Fig 17
(one column)

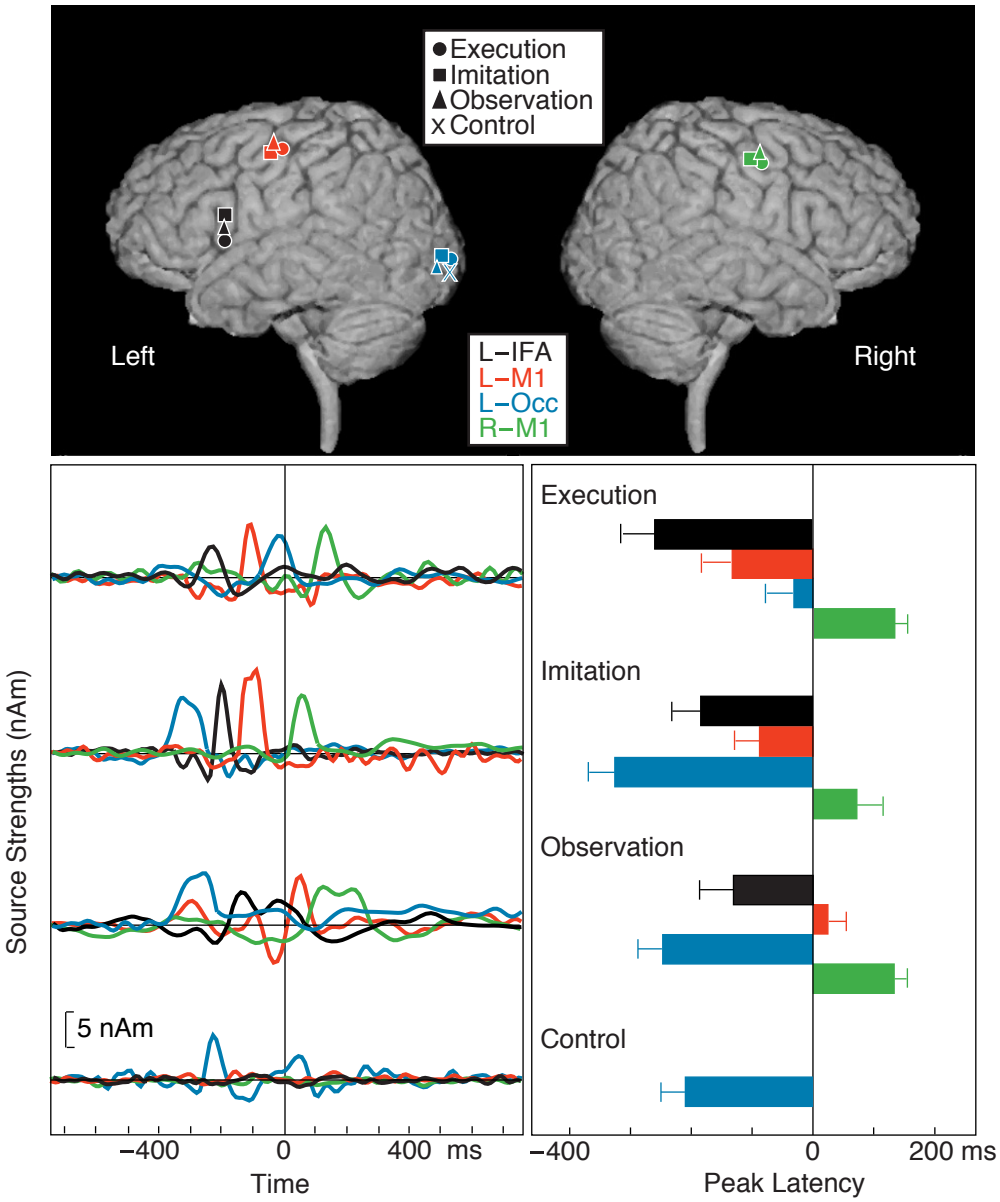

Hämäläinen and Hari, Fig 18

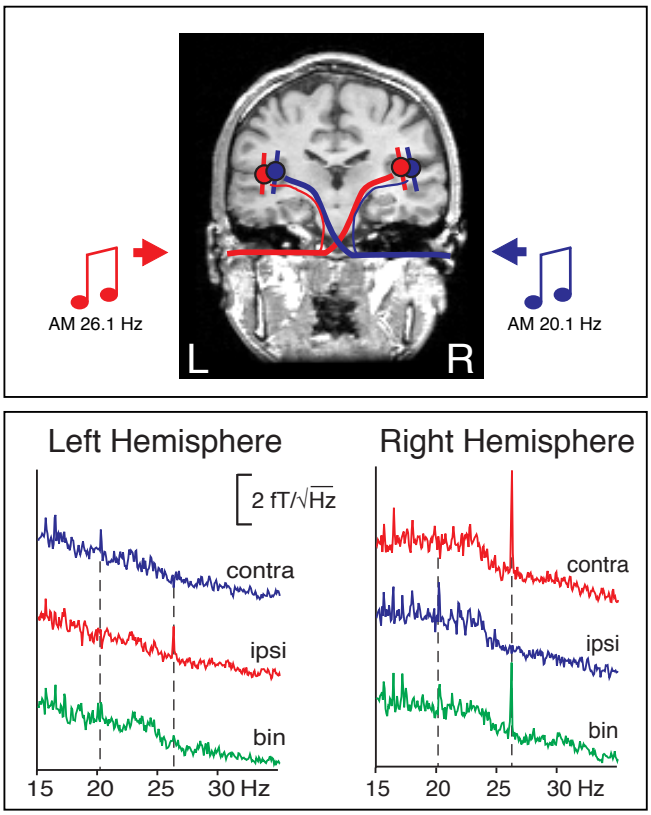

Hämäläinen and Hari, Fig 19□
(one column)

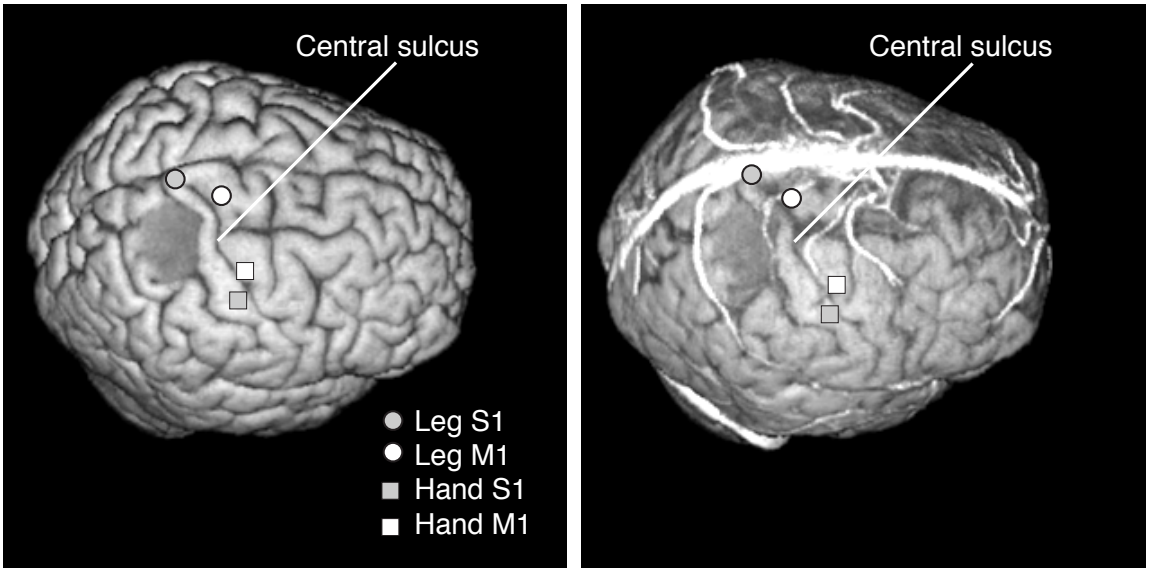

Hämäläinen and Hari, Fig 20